

An Efficient Calculation of Photonic Crystal Band Structures Using Taylor Expansions

Dirk Klindworth* and Kersten Schmidt

*Research Center MATHEON, TU Berlin, Department of Mathematics, Straße des
17. Juni 136, 10623 Berlin, Germany.*

Received 24 May 2013; Accepted (in revised version) 26 June 2014

Available online 2 September 2014

Abstract. In this paper we present an efficient algorithm for the calculation of photonic crystal band structures and band structures of photonic crystal waveguides. Our method relies on the fact that the dispersion curves of the band structure are smooth functions of the quasi-momentum in the one-dimensional Brillouin zone. We show the derivation and computation of the group velocity, the group velocity dispersion, and any higher derivative of the dispersion curves. These derivatives are then employed in a Taylor expansion of the dispersion curves. We control the error of the Taylor expansion with the help of a residual estimate and introduce an adaptive scheme for the selection of nodes in the one-dimensional Brillouin zone at which we solve the underlying eigenvalue problem and compute the derivatives of the dispersion curves. The proposed algorithm is not only advantageous as it decreases the computational effort to compute the band structure but also because it allows for the identification of crossings and anti-crossings of dispersion curves, respectively. This identification is not possible with the standard approach of solving the underlying eigenvalue problem at a discrete set of values of the quasi-momentum without taking the mode parity into account.

AMS subject classifications: 35Q61, 65N30, 65Z05, 78-04, 78M10

PACS: 42.70.Qs, 71.20.-b, 02.30.Jr, 02.70.Dh

Key words: Photonic crystals, band structure calculation, group velocity, Taylor expansion, adaptivity.

1 Introduction

Photonic crystals (PhCs) are nanostructures with a periodic refractive index, where the periodicity is in the order of the wavelength of light [19]. In general one has to distinguish between 1D, 2D, and 3D PhCs, where the number of the dimension stands for the

*Corresponding author. *Email addresses:* dirk.klindworth@math.tu-berlin.de (D. Klindworth), kersten.schmidt@math.tu-berlin.de (K. Schmidt)

number of axes of periodicity. In this work we shall focus on 2D PhCs whose periodicity is usually induced by periodically spaced holes in a dielectric material, or by periodically spaced rods of a dielectric material. A typical approximation, the so called *2D planar PhC*, of this three dimensional structure is obtained by assuming invariance along the direction of the holes and rods. Due to their ability to tailor the propagation of light, 2D PhCs and their band structures, *i.e.* eigenfrequencies in dependence of the quasi-momentum, have been studied extensively, see for example [2–4, 6, 10, 13, 15–18, 24, 26–28] and the references therein. Of particular interest in PhC band structure calculations is the identification of frequency intervals, so called *band gaps* or *complete band gaps*, for which no light can propagate in the PhC. These band gaps are relevant for *PhC waveguides*. PhC waveguides are PhCs with a line defect, that is usually induced by omitting one (W1 PhC waveguide), two (W2 PhC waveguide), or more rows of holes/rods [19]. Inside the band gaps there can exist modes, so called *guided modes*, that propagate along the line defect while decaying exponentially in perpendicular direction.

In the design process of devices in photonics the calculation of band structures of PhC waveguides is a key issue. The frequently used supercell method [35,38] is a simple procedure for the approximative computation of guided modes in PhC waveguides. While giving good results for well-confined modes (guided modes with a large decay rate in perpendicular direction to the line defect), the supercell methods lacks accuracy for modes that are close to the boundaries of the band gaps, the so called *band edges*, since the decay rate for these modes is significantly smaller [38]. Very recently, an approach for an exact computation of guided modes in PhC waveguides was proposed that uses Dirichlet-to-Neumann (DtN) transparent boundary conditions at the interfaces of periodic medium and line defect [11]. A numerical realization and comparison to the supercell method was shown in [22]. This DtN method does not introduce any modelling error and hence, it is also suited for guided modes close to the band edges.

A full band structure calculation, that resolves all phenomena like *crossings* and *anti-crossings* [30,31] of dispersion curves in full detail, is very time-consuming with either method and there is a need for efficient yet reliable methods that provide good approximations to both, well-confined modes and modes close to the band edge. We propose in this work a method that is based on the fact that the dispersion curves in band structures are smooth functions and hence, a Taylor expansion of these functions is possible. We show how to compute the first derivative of the dispersion curves, which corresponds to the so called *group velocity* [5,20], the second derivative, known as *group velocity dispersion*, and any higher derivative of the dispersion curves. The computation of the derivatives relies directly on the differentiability of the underlying operator of the eigenvalue problem with respect to the quasi-momentum. In particular, we do not employ the perturbation theory as done in earlier works [9,14,37], where the vector $\mathbf{k} \cdot \mathbf{p}$ approach of electronic band structure theory is transferred to PhC band structure calculations. Our computational procedure has two main advantages: (i) it is “exact” in the way that no additional modelling error is introduced in comparison to the perturbation approach in [9, 14, 37] where an infinite sum for the computation of the group velocity dispersion has to be

truncated, and (ii) it allows for a successive computation of derivatives up to any order with marginal extra computational costs for each additional order. We then use these derivatives of the dispersion curves in a (piecewise) Taylor expansion of the band structure.

This Taylor expansion can be understood as eigenvalue continuation technique. The homotopy method, see for example [7, 25], is a well established technique to follow so called eigenpaths, *i. e.* dispersion curves in our context. The advantage of our approach is, however, that the Taylor expansion can be computed up to any order, since closed formulas for the derivatives of the dispersion curves up to any order are available, while the homotopy method is, in general, a first order method, that does not take higher derivatives into account.

This paper is organized as follows: In Section 2 we describe the model problem and discuss the differentiability of dispersion curves and the associated eigenmodes with respect to the quasi-momentum. The formulas for the group velocity and any higher derivative of the dispersion curves are presented in Section 3. We employ these derivatives in Section 4 where we propose a Taylor expansion of the dispersion curves and present first numerical results. Then we propose an adaptive algorithm for the band structure calculation in Section 5 and test this algorithm numerically in Section 6. In Section 7 we give concluding remarks. The proof of the piecewise differentiability of the eigenmodes with respect to the quasi-momentum is provided in Appendix A, and in Appendix B we present the formulas for the group velocity and higher derivatives of the dispersion curves for the case with DtN transparent boundary conditions.

2 Model problem

Modes in PhCs and guided modes in PhC waveguides are eigensolutions of the time-harmonic Maxwell's equations [19]. In 2D the electric and magnetic fields of the Maxwell's equation decouple into a *transverse magnetic* (TM) and a *transverse electric* (TE) mode that satisfy a 2D Helmholtz equation. In this work we shall consider both modes and choose

$$-\nabla \cdot \alpha(\mathbf{x}) \nabla U(\mathbf{x}) - \omega^2 \beta(\mathbf{x}) U(\mathbf{x}) = 0, \quad \mathbf{x} \in \mathbb{R}^2, \quad (2.1)$$

as our governing equation. In the TM mode, U describes the electric field in x_3 -direction and the coefficients $\alpha(\mathbf{x})$ and $\beta(\mathbf{x})$ are determined through $\alpha(\mathbf{x}) \equiv 1$ and $\beta(\mathbf{x}) = \varepsilon(\mathbf{x})/c^2$. On the other hand, in the TE mode, U denotes the magnetic field in x_3 -direction and the coefficients are defined by $\alpha(\mathbf{x}) = 1/\varepsilon(\mathbf{x})$ and $\beta(\mathbf{x}) \equiv 1/c^2$. Note that, for simplicity of notation, the velocity of light c is incorporated in the coefficient β .

The function $\varepsilon \in L^\infty(\mathbb{R}^2)$ denotes the relative permittivity of the involved materials. We assume that $\varepsilon(\mathbf{x})$ is real, positive, and bounded from below and above, *i. e.* there exist $\varepsilon_a, \varepsilon_b > 0$ such that $0 < \varepsilon_a < \varepsilon(\mathbf{x}) < \varepsilon_b$ for almost all $\mathbf{x} \in \mathbb{R}^2$. Moreover we assume that it fulfills the periodicity condition $\varepsilon(\mathbf{x} + \mathbf{a}_1) = \varepsilon(\mathbf{x})$, and — in the case of a PhC (in contrast to a PhC waveguide) — also $\varepsilon(\mathbf{x} + \mathbf{a}_2) = \varepsilon(\mathbf{x})$, see Fig. 1.

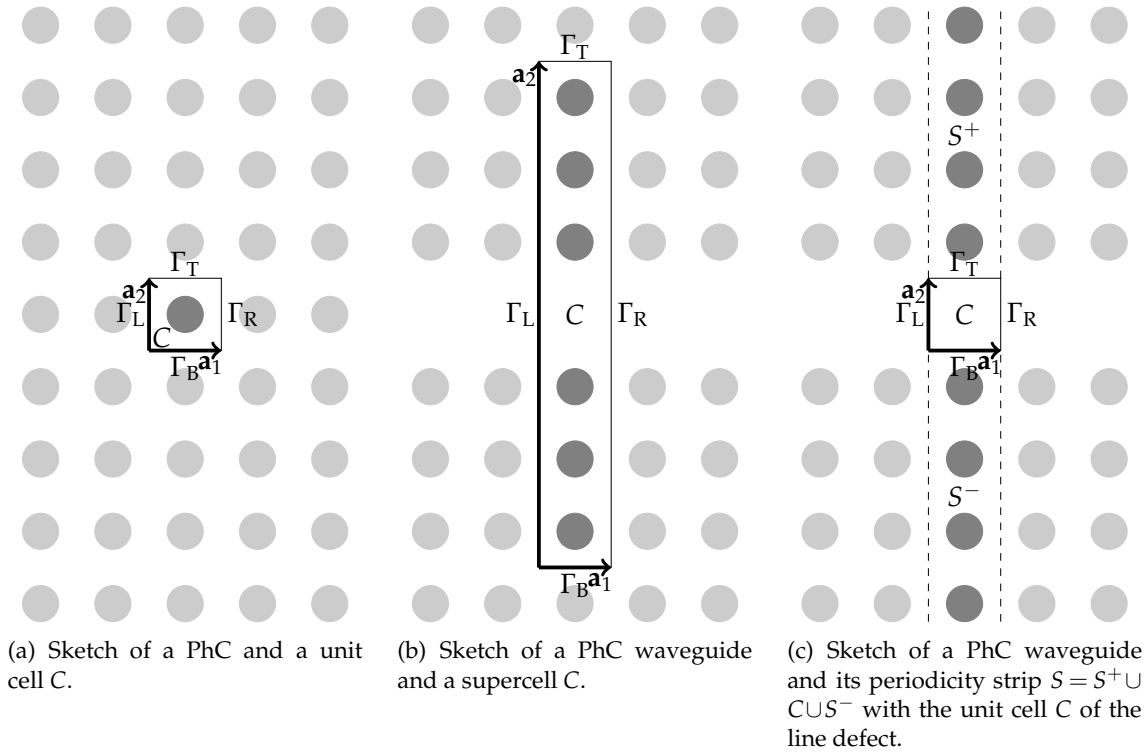


Figure 1: Sketches of the computational domains C , i. e. of the unit cell of a PhC (a), a supercell of a PhC waveguide (b), and a unit cell of the line defect of a PhC waveguide (c) with their boundaries Γ_L , Γ_R , Γ_T and Γ_B , and periodicity vectors \mathbf{a}_1 and \mathbf{a}_2 .

Considering the periodicity of the permittivity in the x_1 -direction, applying the Floquet-Bloch theory [23], and introducing the quasi-momentum $k \in B$ with the one-dimensional Brillouin zone $B = [-\pi/|\mathbf{a}_1|, \pi/|\mathbf{a}_1|]$ the problem (2.1) is equivalent to the problem of finding *Bloch modes* $U(\mathbf{x};k)$ and associated eigenvalues $\omega^2(k) \in \mathbb{R}$ that satisfy

$$-\nabla \cdot \alpha(\mathbf{x}) \nabla U(\mathbf{x};k) - \omega^2(k) \beta(\mathbf{x}) U(\mathbf{x};k) = 0$$

in the computational domain $C \subset \mathbb{R}^2$, which is

- (a) the unit cell of a PhC (see Fig. 1(a)),
- (b) a supercell of a PhC waveguide (see Fig. 1(b)), or
- (c) the unit cell of the line defect of a PhC waveguide (see Fig. 1(c)).

At the left and right boundaries Γ_L and Γ_R of C the Bloch modes satisfy the quasi-periodic boundary conditions

$$U|_{\Gamma_R} = e^{ik|\mathbf{a}_1|} U|_{\Gamma_L}, \quad \partial_{\mathbf{n}} U|_{\Gamma_R} = -e^{ik|\mathbf{a}_1|} \partial_{\mathbf{n}} U|_{\Gamma_L},$$

where $\partial_{\mathbf{n}} = \nabla \cdot \mathbf{n}$ denotes the normal derivative with the unit normal vector \mathbf{n} outward to C . On the top and bottom boundaries Γ_T and Γ_B of C we impose

- (a) quasi-periodic boundary conditions with quasi-momentum $k_2 \in [-\pi/|\mathbf{a}_2|, \pi/|\mathbf{a}_2|]$ in the direction of \mathbf{a}_2 ,
- (b) periodic boundary conditions, *i. e.* quasi-periodic with quasi-momentum $k_2 = 0$, (as used in the supercell method for the approximation of guided modes in PhC waveguides, see for example [35]), or
- (c) DtN maps (as used in [22] for the exact computation of guided modes in PhC waveguides).

For simplicity, we shall focus on periodic boundary conditions in this work, but the results can also be applied to the DtN method for which we summarize the results in the appendix.

By substituting $u(\mathbf{x};k) = U(\mathbf{x};k)e^{-ik\mathbf{a}_1 \cdot \mathbf{x}}$, we arrive at a periodic problem that we express in variational sense using the Sobolev space of periodic H^1 -functions in C denoted by $H_{\text{per}}^1(C)$. For any $k \in B$ we seek modes $u(\cdot;k) \in H_{\text{per}}^1(C)$ and eigenvalues $\omega^2(k) \in \mathbb{R}^+$ such that

$$\int_C \alpha(\nabla + ik\mathbf{a}_1)u \cdot (\nabla - ik\mathbf{a}_1)\bar{v} - \omega^2 \beta u \bar{v} \, d\mathbf{x} = 0 \quad (2.2)$$

for all $v \in H_{\text{per}}^1(C)$. For the definition of Sobolev spaces we refer to Section 2.3 in [34].

Before we shall give the main results at the end of this section, we introduce an example that we shall refer to many times in the remainder of this paper.

Example 2.1. We consider the TM mode in a PhC unit cell of square lattice with holes of relative radius $r/|\mathbf{a}_1| = 0.46$ and permittivity $\varepsilon = 1$ that are surrounded by dielectric material of permittivity $\varepsilon = 8$, see Fig. 2. For illustration, the band structure of the TM mode in the reduced Brillouin zone $\tilde{B} = [0, \pi/|\mathbf{a}_1|]$ is presented in Fig. 3. Here and in the sequel, we choose finite elements on curved cells using the C++ library *Concepts* [8,12,36]. If not stated differently, we choose a mesh of the unit square as presented in Fig. 3 with no further refinement, *i. e.* with nine quadrilateral cells, and we set the polynomial degree to five.

Now we give the main results, the proposed method relies on. We start with a well known result on the analyticity of the dispersion curves, for which we shall give a sketch of a proof.

Proposition 2.1. For any $k \in B$, there exists an ordering of the eigenvalues $\omega_m^2(k) \in \mathbb{R}^+$, $m \in \mathbb{N}$, of the eigenvalue problem (2.2) such that the functions $k \mapsto \omega_m(k)$ — the so-called *dispersion curves* — are continuously differentiable to any order.

Proof. This proposition is a direct consequence of the perturbation theory for linear operators [21], and in particular, of the Katō-Rellich theorem, see for example Chapter 12 in [33]. Since the sesquilinear form and the corresponding linear operator are bounded,

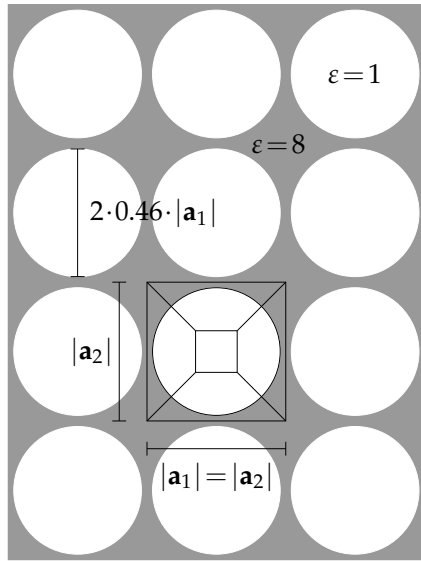


Figure 2: Sketch of the PhC of Example 2.1.

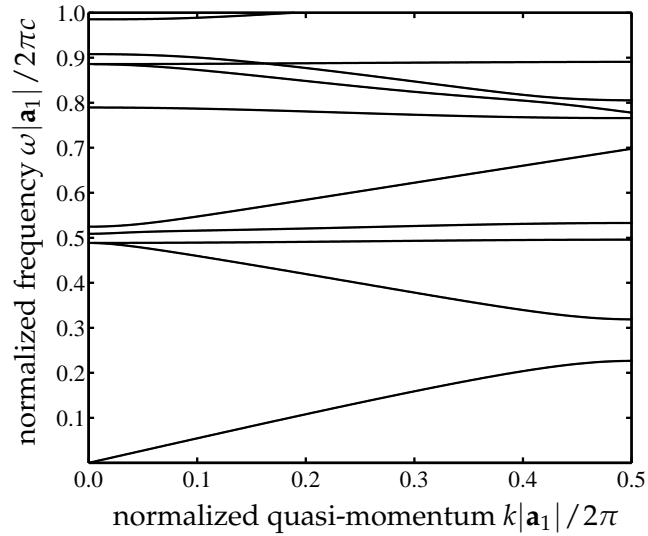


Figure 3: Band structure of Example 2.1.

we conclude that the spectral results of the operator theory directly transfer to the eigenvalue problem (2.2). This is in analogy to Theorem 2 in [29] where the analyticity of the eigenvalues with respect to the quasi-momentum is shown for the Schrödinger equation with periodic potential. \square

In addition to the well known eigenvalue analyticity we now present a similar result for the associated eigenmodes of $\omega_m^2(k)$. The proof can be found in Appendix A.

Proposition 2.2. Let $k_0 \in B$ and let $\omega_m^2(k_0)$ be an eigenvalue of the eigenvalue problem (2.2) with geometric multiplicity one, i. e. the dispersion curve $\omega_m(k)$ does not intersect with any other dispersion curve at $(\omega_m(k_0), k_0)$. Furthermore, let $u_m(\cdot; k_0)$ be a corresponding eigenmode. Then $u_m(\cdot; k_0)$ is continuously differentiable with respect to k at $k = k_0$ up to any order.

We believe that the result also holds true at a crossing of dispersion curves. However, we are not able to provide a proof.

Conjecture 2.1. Let $k_0 \in B$ and let $\omega_m^2(k_0)$ be an eigenvalue of the eigenvalue problem (2.2) with geometric multiplicity $n > 1$, in other words n dispersion curves intersect at $(\omega_m(k_0), k_0)$. Furthermore, let $\{u_{m,1}(\cdot; k_0), \dots, u_{m,n}(\cdot; k_0)\}$ be a set of linearly independent eigenmodes corresponding to $\omega_m^2(k_0)$. Then $u_{m,1}(\cdot; k_0), \dots, u_{m,n}(\cdot; k_0)$ are continuously differentiable with respect to k at $k = k_0$ up to any order.

In the following two remarks we will discuss how to transfer the above results to the case with DtN maps.

Remark 2.1. If we impose DtN maps [22] at the top and bottom boundaries Γ_T and Γ_B , we obtain a non-linear eigenvalue problem, see Eq. (B.1) in Appendix B. If $\omega^2(k)$ is an eigenvalue of (2.2) in the unit cell of the PhC, these DtN maps are not well-defined. If, however, $\omega^2(k)$ is in the band gaps of the PhC and the DtN maps are well-defined, the non-linear problem (B.1) in the defect cell C with DtN maps on the top and bottom boundaries Γ_T and Γ_B is equivalent to the linear problem (2.2) in the infinite strip S [11], see Fig. 1(c) for a sketch of the domain S . Hence, the perturbation theory for linear operators can again be applied. This implies that, in the case with DtN transparent boundary conditions, we additionally need to assume that the eigenvalues $\omega_m^2(k) \in \mathbb{R}^+$ are in the band gaps of the PhC. Note that the ordering has to account for the fact that dispersion curves of guided modes can leave the band gap of the PhC and thus, they may not be defined in B but only in some subinterval of B .

Remark 2.2. Proposition 2.2 also holds true for the case with DtN transparent boundary conditions. The proof is similar and uses the fact that the DtN operators are differentiable with respect to ω and k up to any order [22]. Furthermore, we claim that Conjecture 2.1 is valid also for the case with DtN transparent boundary conditions.

3 Derivatives of the dispersion curves

3.1 First derivative of the dispersion curves — the group velocity

Thanks to Propositions 2.1 and 2.2 and Conjecture 2.1 we can take the derivative of Eq. (2.2) with respect to k and obtain

$$\int_C \alpha(\nabla + i\mathbf{k}\mathbf{a}_1) d_k u \cdot (\nabla - i\mathbf{k}\mathbf{a}_1) \bar{v} - \omega^2 \beta d_k u \bar{v} \, dx = f_1(v) \tag{3.1}$$

for all $v \in H_{\text{per}}^1(C)$, with the short notations $\omega'(k) := \frac{\partial \omega}{\partial k}(k)$ and $d_k u(\cdot; k) := \frac{du}{dk}(\cdot; k) \in H_{\text{per}}^1(C)$, and the linear form

$$\begin{aligned} f_1(v) &= \int_C \alpha(\nabla + i\mathbf{k}\mathbf{a}_1) u \cdot i\mathbf{a}_1 \bar{v} - \alpha i\mathbf{a}_1 u \cdot (\nabla - i\mathbf{k}\mathbf{a}_1) \bar{v} + 2\omega\omega' \beta u \bar{v} \, dx \\ &= -2k|\mathbf{a}_1|^2 \int_C \alpha u \bar{v} \, dx - i|\mathbf{a}_1| \int_C \alpha u (\partial_1 \bar{v}) - \alpha (\partial_1 u) \bar{v} \, dx + 2\omega\omega' \int_C \beta u \bar{v} \, dx. \end{aligned}$$

Taking $v = u$ as test function in Eq. (3.1) we have

$$\begin{aligned} &\int_C \alpha(\nabla + i\mathbf{k}\mathbf{a}_1) d_k u \cdot (\nabla - i\mathbf{k}\mathbf{a}_1) \bar{u} - \omega^2 \beta d_k u \bar{u} \, dx \\ &= -2k|\mathbf{a}_1|^2 \int_C \alpha |u|^2 \, dx - i|\mathbf{a}_1| \int_C \alpha u (\partial_1 \bar{u}) - \alpha (\partial_1 u) \bar{u} \, dx + 2\omega\omega' \int_C \beta |u|^2 \, dx, \end{aligned}$$

where the left hand side including all terms containing $d_k u$ vanishes since $(-k)$ is an eigenvalue of (2.2) with associated eigenmode \bar{u} , which can easily be seen by taking the

complex conjugate of (2.2). On the other hand, — since $\alpha(\mathbf{x}) \in \mathbb{R}$ for all $\mathbf{x} \in C$ — the integral $\int_C \alpha u (\partial_1 \bar{u}) - \alpha (\partial_1 u) \bar{u} \, d\mathbf{x}$ on the right hand side is purely imaginary and hence, using integration by parts and the fact that u is periodic, we can rewrite it in the form

$$\begin{aligned} i \operatorname{Im} \left(\int_C \alpha u (\partial_1 \bar{u}) - \alpha (\partial_1 u) \bar{u} \, d\mathbf{x} \right) &= 2i \operatorname{Im} \left(\int_C \alpha u (\partial_1 \bar{u}) \, d\mathbf{x} \right) + i \operatorname{Im} \left(\int_C (\partial_1 \alpha) |u|^2 \, d\mathbf{x} \right) \\ &= 2i \operatorname{Im} \left(\int_C \alpha u (\partial_1 \bar{u}) \, d\mathbf{x} \right). \end{aligned}$$

Note that the derivative of α , that appears in the above equation, has to be understood in distributional sense and thus, it is well defined even though we assume only $\alpha \in L^\infty(\mathbb{R}^2)$. Moreover, it is obvious, that $\int_C (\partial_1 \alpha) |u|^2 \, d\mathbf{x}$ is well defined since both other integrals of the equation are well defined.

Thus, the group velocity reads

$$\omega'(k) = \frac{k |\mathbf{a}_1|^2 \int_C \alpha |u|^2 \, d\mathbf{x} - |\mathbf{a}_1| \operatorname{Im} \left(\int_C \alpha u \partial_1 \bar{u} \, d\mathbf{x} \right)}{\omega \int_C \beta |u|^2 \, d\mathbf{x}} \quad (3.2)$$

and is real-valued.

Remark 3.1. The formula (3.2) for the group velocity contains the eigenmode u associated to the eigenvalue $\omega^2(k)$. However, the eigenmode is not uniquely defined. If the eigenvalue has multiplicity equal to one, any scalar multiple of an eigenmode is also an eigenmode. However, such a scalar cancels out in (3.2) and the group velocity formula is well-defined. If the eigenvalue has multiplicity larger than one, the situation is more involved. In fact the analyticity of the eigenmodes at crossings has not been proven. Nevertheless, we claim — in accordance to Conjecture 2.1 — that the eigenmodes in (3.2) can be chosen as the limit of the eigenmodes associated to the eigenvalues of multiplicity one, that lie on the dispersion curves which intersect at $(\omega(k), k)$. However, note that from a practical perspective this case is only relevant at $k=0$, since we know that at $k=0$ dispersion curves can intersect and hence, eigenvalues may have multiplicity larger than one. On the other hand, it is very unlikely that a numerical scheme will find the exact location of a crossing at $k \neq 0$.

3.2 Comparison of group velocity formula and difference quotient

Let us now discuss the benefit of the group velocity formula (3.2) in the context of a finite element discretization. According to the Babuška-Osborn theory on eigenvalue problems [1], we expect that — using a finite element discretization — the eigenvectors converge with smaller convergence rate than the eigenvalues when increasing the refinement of the discretization. Hence, we shall analyse the convergence of the group velocity formula (3.2) when increasing the refinement of the discretization and compare this rate of convergence with that one of a difference quotient of the dispersion curve,

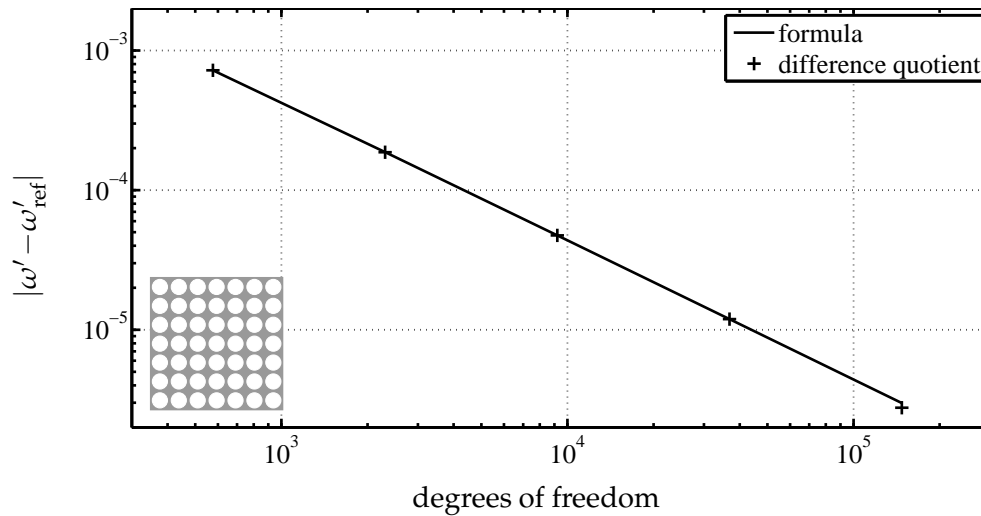


Figure 4: Convergence of the error of the group velocity formula (solid line) and the first order difference quotient (markers) when increasing the grid refinement of a finite element computation with polynomial degree one. The reference solution is computed with polynomial degree 20.

that is an approximation to the group velocity. To this end, let us do a convergence study for the setup in Example 2.1. Fig. 4 shows the convergence of the error of the group velocity formula (3.2) and the (first order) difference quotient of the first dispersion curve at $k = \pi/2|\mathbf{a}_1|$ when increasing the mesh refinement of a finite element discretization of polynomial degree one. The reference solution, on the other hand, is computed with the smallest mesh refinement and with polynomial degree 20. Both, the formula (3.2) for the group velocity as well as the difference quotient converge with the same convergence rate when increasing the refinement of the discretization, which demonstrates that the group velocity formula (3.2) has no disadvantages compared to a difference quotient in a finite element discretization.

3.3 Higher derivatives of the dispersion curves

Using the formula (3.2) for the group velocity ω' , we can deduce that the linear form f_1 only depends on u and is independent of $d_k u$. The solution $d_k u \in H_{\text{per}}^1(C)$ of Eq. (3.1) is not unique since there exist eigenmodes $u \in H_{\text{per}}^1(C)$ that solve Eq. (2.2) with zero right hand side and hence, any of these eigenmodes u can be added to the solution $d_k u$ of Eq. (3.1) and the equation will still be satisfied. However, applying the Fredholm–Riesz–Schauder theory [34], we can compute a particular solution $d_k u$ of Eq. (3.1) by additionally requiring $H^1(C)$ -orthogonality of $d_k u$ and any of the finitely many [10,11], linearly independent eigenmodes $u_j, j = 1, \dots, J$. To simplify the presentation and in accordance to Remark 3.1, we shall assume in the sequel, that the eigenvalue $\omega^2(k)$ has multiplicity one, and hence,

we seek $d_k u \in H^1_{\text{per}}(C)$ and $\lambda \in \mathbb{C}$ such that

$$\int_C \alpha(\nabla + ika_1) d_k u \cdot (\nabla - ika_1) \bar{v} - \omega^2 \beta d_k u \bar{v} \, dx + \lambda \int_C \nabla u \cdot \nabla \bar{v} + u \bar{v} \, dx = f_1(v), \tag{3.3a}$$

$$\int_C \nabla d_k u \cdot \nabla \bar{u} + d_k u \bar{u} \, dx = 0, \tag{3.3b}$$

for all $v \in H^1_{\text{per}}(C)$.

Remark 3.2. From the Fredholm–Riesz–Schauder theory we know that the mixed variational problem (3.3) has a unique solution. The Lagrangian multiplier λ of this unique solution is zero, since, testing (3.3a) with $v = u$, $\|u\|_{H^1(C)} = 1$, yields $\lambda = f_1(u)$, which is identical to zero due to (3.1) and the fact that $(-k)$ is an eigenvalue of (2.2) with associated eigenmode \bar{u} .

In order to determine higher derivatives of $k \mapsto \omega_m(k)$ let us introduce the following short notations

$$d_k^n u(\cdot; k) := \frac{d^n u}{dk^n}(\cdot; k) \quad \text{and} \quad \omega^{(n)}(k) := \frac{\partial^n \omega}{\partial k^n}(k).$$

Taking the n -th derivative of Eq. (2.2) with respect to k yields

$$\int_C \alpha(\nabla + ika_1) d_k^n u \cdot (\nabla - ika_1) \bar{v} - \omega^2 \beta d_k^n u \bar{v} \, dx = f_n(v)$$

for all $v \in H^1_{\text{per}}(C)$, where the linear form f_n , that is obtained using binomial and trinomial expansions, reads

$$\begin{aligned} f_n(v) = & \sum_{p=0}^{n-1} \sum_{q=0}^{n-p} \frac{n!}{p!q!(n-p-q)!} \omega^{(n-p-q)} \omega^{(q)} \int_C \beta d_k^p u \bar{v} \, dx \\ & - in|a_1| \int_C \alpha d_k^{n-1} u (\partial_1 \bar{v}) - \alpha (\partial_1 d_k^{n-1} u) \bar{v} \, dx \\ & - 2nk|a_1|^2 \int_C \alpha d_k^{n-1} u \bar{v} \, dx - n(n-1)|a_1|^2 \int_C \alpha d_k^{n-2} u \bar{v} \, dx. \end{aligned} \tag{3.4}$$

From this we deduce the n -th derivative of $\omega(k)$

$$\begin{aligned} \omega^{(n)} = & \frac{1}{2\omega \int_C \beta |u|^2 \, dx} \left(n(n-1)|a_1|^2 \int_C \alpha d_k^{n-2} u \bar{u} \, dx + 2nk|a_1|^2 \int_C \alpha d_k^{n-1} u \bar{u} \, dx \right. \\ & + in|a_1| \int_C \alpha d_k^{n-1} u (\partial_1 \bar{u}) - \alpha (\partial_1 d_k^{n-1} u) \bar{u} \, dx \\ & - \sum_{p=1}^{n-1} \sum_{q=0}^{n-p} \frac{n!}{p!q!(n-p-q)!} \omega^{(n-p-q)} \omega^{(q)} \int_C \beta d_k^p u \bar{u} \, dx \\ & \left. - \sum_{q=1}^{n-1} \frac{n!}{q!(n-q)!} \omega^{(n-q)} \omega^{(q)} \int_C \beta |u|^2 \, dx \right). \end{aligned} \tag{3.5}$$

Analogously to above — using the Lagrangian multiplier $\lambda \in \mathbb{C}$ — we can then compute the particular solution $d_k^n u \in H_{\text{per}}^1(C)$ that satisfies

$$\begin{aligned} \int_C \alpha(\nabla + ika_1) d_k^n u \cdot (\nabla - ika_1) \bar{v} - \omega^2 \beta d_k^n u \bar{v} \, dx + \lambda \int_C \nabla u \cdot \nabla \bar{v} + u \bar{v} \, dx &= f_n(v) \\ \int_C \nabla d_k^n u \cdot \nabla \bar{u} + d_k^n u \bar{u} \, dx &= 0 \end{aligned} \tag{3.6}$$

for all $v \in H_{\text{per}}^1(C)$, which is, for $n = 1$, equivalent to Eq. (3.3). Note that the terms on left hand side of Eq. (3.6) are identical for all $n \in \mathbb{N}$ but the source terms $f_n(v)$ on the right hand side differ.

In order to compute $\omega^{(n)}$ we have to solve (2.2) for its eigenvalue $\omega^2(k)$ and associated eigenmode u . Then we successively compute $\omega^{(l)}$ from (3.5) and solve the linear system (3.6) for $d_k^l u$, $l = 1, \dots, n - 1$. Finally, it remains to compute $\omega^{(n)}$ from (3.5). In total we have to solve one eigenvalue problem (2.2), $n - 1$ linear systems (3.6), and n algebraic equations (3.5).

If there are multiple, linearly independent eigenmodes $u_{m,j}$, $j = 1, \dots, J$, associated to the eigenvalue $\omega_m^2(k)$ of (2.2), $J - 1$ extra orthogonality conditions and Lagrangian multipliers $\lambda_2, \dots, \lambda_J \in \mathbb{C}$ have to be added to the linear system (3.6). Note that these eigenmodes $u_{m,j}$ have to be selected as described in Remark 3.1, *i. e.* as the limit of the eigenmodes corresponding to the eigenvalues of multiplicity one in the vicinity of $\omega_m^2(k)$. The procedure to compute the n -th derivative $\omega_{m,j}^{(n)}$ of $\omega_m(k)$ associated to $u_{i,j}$ remains the same, only that we have to bear in mind that each eigenmode $u_{m,j}$ associated to the eigenvalue $\omega_m^2(k)$ yields different quantities $d_k^n u_{m,j}$ and $\omega_{m,j}^{(n)}$.

In practise, these extra orthogonality conditions need to be added to the system (3.6) also in a small vicinity of an eigenvalue with multiplicity larger than one, since the condition number of the matrix related to the linear system (3.6) increases dramatically near such an eigenvalue. The size of this vicinity is subject to numerical testing. We observed that reasonably good results can be obtained if orthogonality conditions for all eigenvalues $\omega^2(k)$ with distance to $\omega_m^2(k)$ smaller than 10^{-2} are added to (3.6).

4 Taylor expansion of the dispersion relation

In this section we explain and demonstrate how to employ the derivatives $\omega^{(n)}(k)$, $n \in \mathbb{N}$, in a Taylor expansion of the dispersion relation.

4.1 Taylor expansion of analytic functions

Since the dispersion curves $k \mapsto \omega_m(k)$ are continuously differentiable to any order we can apply the Taylor theorem, and hence, for any $k_0 \in B$ and $n \in \mathbb{N}$

$$\omega(k) = \sum_{i=0}^n \frac{(k-k_0)^i}{i!} \omega^{(i)}(k_0) + R_n(k), \quad k \in B, \quad (4.1)$$

with the remainder

$$R_n(k) = \frac{1}{n!} \int_{k_0}^k (k-\kappa)^n \omega^{(n+1)}(\kappa) d\kappa.$$

The formula (4.1) can be used to approximate the dispersion relation

$$\omega(k) \approx \sum_{m=0}^n \frac{(k-k_0)^m}{m!} \omega^{(m)}(k_0),$$

where the eigenvalue problem (2.2) only has to be solved for k_0 and the derivatives $\omega^{(n)}(k_0)$ have to be computed according to the procedure described in the previous section. Taylor expansions of analytic functions are known to converge in a vicinity of k_0 but not necessarily in the whole Brillouin zone.

4.2 Numerical results of the Taylor expansion of a photonic crystal band structure

For illustration we will now show numerical results for Example 2.1. We study the TM mode in the reduced Brillouin zone $\widehat{B} = [0, \pi/|\mathbf{a}_1|]$ and compare the dispersion relation $\omega(k)$ at 40 values of k with the results of the Taylor expansion around the centre $k_0 = \pi/2|\mathbf{a}_1|$ of the reduced Brillouin zone \widehat{B} .

In Fig. 5 we present a comparison of the Taylor expansion of orders $n = 3$ and $n = 20$ with the “exact” sixth and seventh dispersion curve. We can see from Fig. 5(a) that already a Taylor expansion of order $n = 3$ provides a good approximation of the sixth dispersion curve (red line). For the presented level of detail, we can only see a difference of the Taylor expansion and the exact curve near $k = \pi/|\mathbf{a}_1|$. The seventh dispersion curve (blue line) is also well approximated in a vicinity of the centre $k_0 = \pi/2|\mathbf{a}_1|$ of the expansion but the error increases towards the borders of \widehat{B} , *i. e.* where $|k - k_0|$ becomes large.

However, increasing the order n of the Taylor expansion does not lead to lower error levels near the end points as can be seen in Fig. 5(b) where the Taylor expansion of order $n = 20$ is shown. While the approximation error of the sixth dispersion curve decreases, the approximation error of the seventh dispersion curve becomes even larger near $k = 0$ and $k = \pi/|\mathbf{a}_1|$. This can be explained by analysing the behaviour of the remainder R_n . But before we do so, we present the convergence of the Taylor expansion. In Fig. 6 the maximum errors over a set of 40 equidistant values of $k \in \widehat{B}$ of the Taylor expansion of the sixth and seventh dispersion curves are plotted with respect to the order n of the Taylor expansion. While we observe exponential convergence of the error of the sixth dispersion curve, the error of the seventh dispersion curve diverges when increasing the order n .

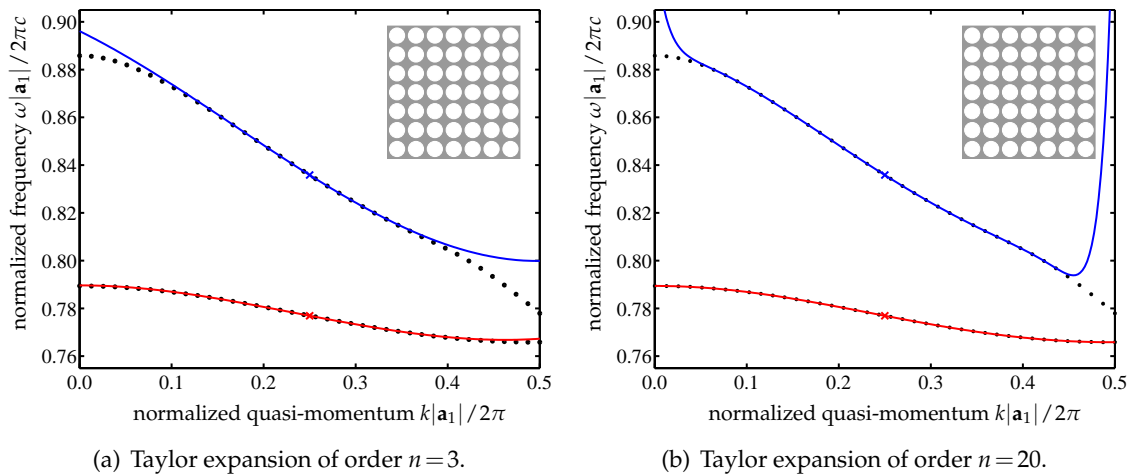


Figure 5: Sixth (red) and seventh (blue) dispersion curves of Example 2.1. Taylor expansion (solid lines) of order $n=3$ (left) and $n=20$ (right) around $k_0=\pi/2|a_1|$ (crosses) compared to “exact” dispersion curves (dotted lines) evaluated at 40 equidistant values of k .

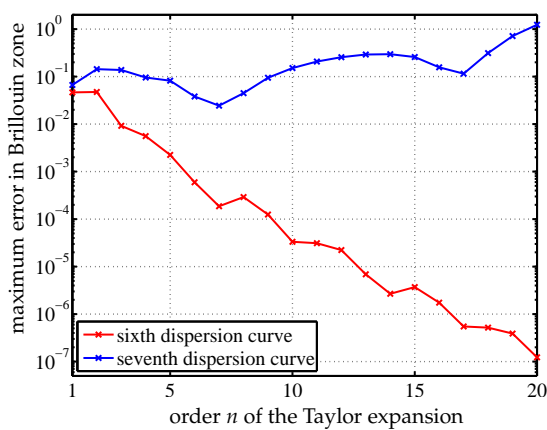


Figure 6: Maximum error of the Taylor expansion of the sixth (red) and seventh (blue) dispersion curve of the band structure presented in Figure 5 in dependence on the order n of the Taylor expansion. The maximum error is evaluated on an equidistant grid of 40 values of $k \in \hat{B}$.

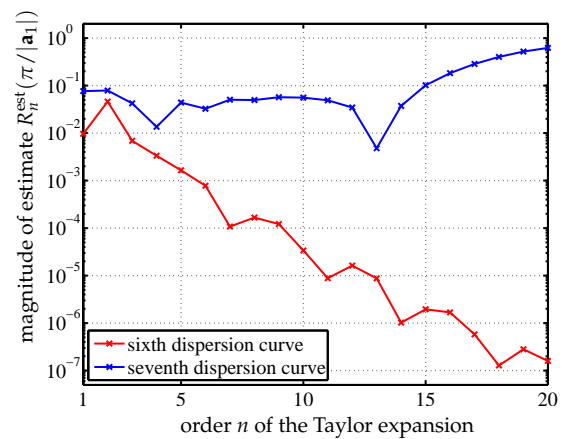


Figure 7: Magnitude of the non-rigorous estimate $R_n^{\text{est}}(k)$ of the remainder $R_n(k)$ at $k=\pi/|a_1|$ of the Taylor expansion of the sixth (red) and seventh (blue) dispersion curve around $k_0=\pi/2|a_1|$ of the band structure presented in Fig. 5 in dependence on the order n of the Taylor expansion.

4.3 Estimation of the remainder

Now let us study the behaviour of the remainder R_n in order to explain the behaviour of the Taylor expansion of the seventh dispersion curve when increasing the order n . To

this end, we first derive an estimate of the remainder R_n . Without loss of generality let $k > k_0$. According to the mean value theorem for integration, there exists $\hat{k} \in [k_0, k]$ such that the remainder satisfies

$$R_n(k) = \frac{1}{n!} \omega^{(n+1)}(\hat{k}) \int_{k_0}^k (k-\kappa)^n d\kappa = \frac{(k-k_0)^{n+1}}{(n+1)!} \omega^{(n+1)}(\hat{k}), \quad (4.2)$$

which is known as the Lagrange form of the remainder. Clearly,

$$R_n^{\text{UB}}(k) = \frac{(k-k_0)^{n+1}}{(n+1)!} \max_{\kappa \in [k_0, k]} \omega^{(n+1)}(\kappa) \quad (4.3)$$

is an upper bound for $R_n(k)$, while

$$R_n^{\text{LB}}(k) = \frac{(k-k_0)^{n+1}}{(n+1)!} \min_{\kappa \in [k_0, k]} \omega^{(n+1)}(\kappa)$$

is a lower bound for $R_n(k)$. Hence, a simple, non-rigorous estimate for the remainder $R_n(k)$ is given by

$$R_n^{\text{est}}(k) = \frac{(k-k_0)^{n+1}}{(n+1)!} \omega^{(n+1)}(k_0). \quad (4.4)$$

In Fig. 7 this estimate is presented for the sixth and seventh dispersion curve of the example introduced above. The estimate is evaluated at $k = \pi/|\mathbf{a}_1|$, *i. e.* the distance $|k - k_0|$ is maximal. We can see that the estimate $R_n^{\text{est}}(k)$ of the sixth dispersion curve decreases with the order n which is in correspondence to the decrease of the actual maximum error presented in Fig. 6. The estimate $R_n^{\text{est}}(k)$ of the seventh dispersion curve, however, increases with the order n which explains the increasing error of the Taylor expansion that can be observed in Fig. 5. In other words, the derivatives $\omega^{(n)}$ increase faster with n than the ratio $n!/|k - k_0|^n$. This means that we have to restrict the computation of the Taylor expansion to a vicinity of k_0 such that $|k - k_0|^n$ is sufficiently small and hence, the ratio $|k - k_0|^{n+1}/(n+1)!$ dominates the estimate $R_n^{\text{est}}(k)$. For example, if we want the error of the Taylor expansion to be (roughly) smaller than some error tolerance $\varepsilon_{\text{tol}}^{\text{step}}$ we restrict our expansion to the domain $[k_0 - k_{h,n}(k_0), k_0 + k_{h,n}(k_0)]$, where the step size $k_{h,n}(k_0)$ is obtained from

$$k_{h,n}(k_0) = \left(\varepsilon_{\text{tol}}^{\text{step}} \frac{(n+1)!}{|\omega^{(n+1)}(k_0)|} \right)^{\frac{1}{n+1}}. \quad (4.5)$$

The quality of the non-rigorous estimate $R_n^{\text{est}}(k)$ of the remainder can be seen from a comparison of Figs. 6 and 7. We can see that the maximum error in Fig. 6 behaves very similar to the estimate of the remainder in Fig. 7. In fact the effectivity of the estimate, *i. e.* the ratio of estimate and maximum error, varies between 0.21 ($n=1$) and 1.31 ($n=6$) for the sixth dispersion curve, and between 0.02 ($n=13$) and 2.48 ($n=17$) for the seventh dispersion curve, and is hence, reasonably close to one.

Another estimate of the remainder, that reduces the underestimation of the actual maximum error, can be obtained when we additionally estimate the derivative $\omega^{(n+1)}(\kappa)$ in Eq. (4.3) by its Taylor expansion of, *e. g.*, first order. In other words, we do not estimate the maximum of $\omega^{(n+1)}(\kappa)$ in the interval $[k_0, k]$ by $\omega^{(n+1)}(k_0)$ as done in Eq. (4.4), but

$$\begin{aligned} \max_{\kappa \in [k_0, k]} \omega^{(n+1)}(\kappa) &\approx \max_{\kappa \in [k_0, k]} \left(\omega^{(n+1)}(k_0) + (\kappa - k_0) \omega^{(n+2)}(k_0) \right) \\ &= \max \left\{ \omega^{(n+1)}(k_0), \omega^{(n+1)}(k_0) + (k - k_0) \omega^{(n+2)}(k_0) \right\}, \end{aligned}$$

and similarly

$$\begin{aligned} \min_{\kappa \in [k_0, k]} \omega^{(n+1)}(\kappa) &\approx \min_{\kappa \in [k_0, k]} \left(\omega^{(n+1)}(k_0) + (\kappa - k_0) \omega^{(n+2)}(k_0) \right) \\ &= \min \left\{ \omega^{(n+1)}(k_0), \omega^{(n+1)}(k_0) + (k - k_0) \omega^{(n+2)}(k_0) \right\}, \end{aligned}$$

This new estimate

$$\begin{aligned} \tilde{R}_n^{\text{est}}(k) &= \text{sign} \left(\omega^{(n+1)}(k_0) \right) \frac{(k - k_0)^{n+1}}{(n+1)!} \\ &\quad \times \max \left\{ \left| \omega^{(n+1)}(k_0) \right|, \left| \omega^{(n+1)}(k_0) + (k - k_0) \omega^{(n+2)}(k_0) \right| \right\} \end{aligned} \quad (4.6)$$

reduces the underestimation of the actual maximum error. In fact, the effectivity of the estimate $\tilde{R}_n^{\text{est}}(k)$ varies between 0.97 ($n=2$) and 12.07 ($n=14$) for the sixth dispersion curve, and between 0.40 ($n=12$) and 68.63 ($n=17$) for the seventh dispersion curve. Thus, the reduction of the underestimation comes with the price of an increasing overestimation for certain orders.

The computation of the acceptable step size $\tilde{k}_{h,n}(k_0)$ based on the estimate $\tilde{R}_n^{\text{est}}(k_0)$ of the remainder is slightly more complicated than the computation of $k_{h,n}(k_0)$ in Eq. (4.5) since $(k - k_0)$ appears in Eq. (4.6) not only to the power $(n+1)$ as before, but also to the power $(n+2)$. Hence, we have to find the roots $\kappa_h > 0$ of

$$\frac{\kappa_h^{n+1}}{(n+1)!} \left| \omega^{(n+1)}(k_0) + \kappa_h \omega^{(n+2)}(k_0) \right| - \varepsilon_{\text{tol}}^{\text{step}} = 0 \quad (4.7)$$

using, *e. g.*, Newton's method, and then we choose

$$\tilde{k}_{h,n}(k_0) = \min \{ k_{h,n}(k_0), \kappa_h \}. \quad (4.8)$$

5 An adaptive approximation of the dispersion relation

We first propose a simple algorithm for the computation of an approximation to a dispersion curve $\omega(k)$, $k \in \hat{B} = [0, \pi / |\mathbf{a}_1|]$. We start by choosing an error tolerance $\varepsilon_{\text{tol}}^{\text{step}}$ for the step

size, and an order n of the Taylor expansion. Then we set $k^{(0)} = \pi / (2|\mathbf{a}_1|)$ and compute a set of eigenvalues $\omega^2(k^{(0)})$. In case of the supercell approximation of guided modes in PhC waveguides we omit eigenvalues outside the band gaps, *i. e.* at frequencies where propagating PhC modes exist. For each eigenvalue we proceed as follows: We determine the acceptable step size $k_{h,n}(k_0^{(1)})$ according to (4.5). If $k_{h,n}(k^{(0)}) \geq \pi / (2|\mathbf{a}_1|)$ we approximate $\omega(k)$ by its Taylor expansion in the whole reduced Brillouin zone \hat{B} . Otherwise, we set $k^{(-1)} = k^{(0)} - k_{h,n}(k^{(0)})$ and $k^{(+1)} = k^{(0)} + k_{h,n}(k^{(0)})$, and compute the eigenvalues $\omega^2(k^{(-1)})$ and $\omega^2(k^{(+1)})$ which are closest to their estimation that is obtained by a Taylor expansion of order n around $k^{(0)}$ at $k^{(-1)}$ and $k^{(+1)}$, respectively. Then we compute the acceptable step sizes $k_{h,n}(k^{(\pm 1)})$. We continue with this procedure until $k^{(-p)} - k_{h,n}(k^{(-p)}) \leq 0$ and $k^{(+q)} + k_{h,n}(k^{(+q)}) \geq \pi / |\mathbf{a}_1|$, for some $p, q \in \mathbb{N}$. We take the values ω and their derivatives $\omega^{(i)}$, $i = 1, \dots, n$, at $k^{(j)}$, $j = -p, \dots, q$ and compute an approximation to the dispersion curve using, *e. g.*, an Hermite interpolation [32] or a weighted Taylor expansion where we approximate

$$\omega(k) \approx \frac{k^{(j+1)} - k}{k^{(j+1)} - k^{(j)}} \sum_{i=0}^n \frac{(k - k^{(j)})^i}{i!} \omega^{(i)}(k^{(j)}) + \frac{k - k^{(j)}}{k^{(j+1)} - k^{(j)}} \sum_{i=0}^n \frac{(k - k^{(j+1)})^i}{i!} \omega^{(i)}(k^{(j+1)}), \quad (5.1)$$

if $k \in [k^{(j)}, k^{(j+1)}]$, $j = -p, \dots, q-1$, and in the intervals $[0, k^{(-p)}]$ and $[k^{(+q)}, \pi / |\mathbf{a}_1|]$ we take the Taylor expansion directly. The former approach has the advantage that it delivers a smooth curve while the latter approach comes with negligible additional costs.

The computational effort of this algorithm is as follows: In addition to the eigenvalue problem (2.2) at the start value $k^{(0)}$, we have to solve for each dispersion curve a total of $p+q$ eigenvalue problems (2.2), $n(p+q+1)$ linear systems (3.6) and $(n+1)(p+q+1)$ algebraic equations (3.5). For each of the $p+q+1$ values of k we have to compute the acceptable step size using Eq. (4.5), which is a simple scalar equation, or using Eq. (4.8), for which we also have to solve the non-linear equation (4.7) and require derivatives of order $n+2$, *i. e.* we have to replace n by $n+1$ in the formulas for the computational complexity given above.

Now let us introduce two additional refinement checks that will help to improve our approximation.

Backward check An improvement of the adaptive scheme can be realized by a backward check, *i. e.* we check if the Taylor expansion around $k^{(j\pm 1)}$ recovers the original value $\omega(k^{(j)})$ plus/minus some tolerance $\varepsilon_{\text{tol}}^{\text{bwd}}$. If not, it is possible that we mistakenly switched to another dispersion curve or the acceptable step size at $k^{(j\pm 1)}$ is much smaller than at $k^{(j)}$. Then we refine the step size $k_{h,n}(k^{(j)})$, *i. e.* we multiply it by a factor smaller than one, *e. g.*, $1/2$. When carrying out the backward check we also have to solve the eigenvalue problem (2.2) and compute the frequency derivatives at the borders of the reduced Brillouin zone at $k=0$ and $k = \pi / |\mathbf{a}_1|$ such that the Taylor expansions around $k^{(-p)}$ and $k^{(+q)}$ can be validated.

Mini-stop band check A special emphasis in the band structure calculation has to be put into the question whether two dispersion curves cross or anti-cross and form a so called *mini-stop band* [31]. It is well known, that for symmetric waveguides (*e.g.* W1 waveguides with square or hexagonal lattice) modes of opposite parity cross while modes of identical parity form a mini-stop band. On the other hand, for waveguides, whose holes/rods on top of the line defect are shifted exactly by $|\mathbf{a}_1|/2$ compared to the holes/rods below the guide (*e.g.* W2 waveguide with hexagonal lattice) just the opposite holds true: modes of identical parity cross while modes of opposite parity form a mini-stop band. If the waveguide does not satisfy either of these conditions (*e.g.* the shift is less than $|\mathbf{a}_1|/2$), all modes anti-cross and form very narrow mini-stop bands [30]. Even though this classification allows for an identification of crossings and anti-crossings, we will propose here a mini-stop band check that allows to identify mini-stop bands without comparing the parities of the modes.

After two dispersion curves were approximated with the described adaptive scheme and it turned out that the approximated dispersion curves cross at some point k_0 , say, we solve the eigenvalue problem (2.2) at k_0 where we will obtain two close eigenvalues near the expected crossing. Note that, also if the expected crossing turns out to be an actual crossing, these two eigenvalues are most likely not identical but only very close. Then we compute the group velocities of these two eigenmodes at k_0 using the formula (3.2) and compare them with the first derivatives of the approximated dispersion curves (5.1). If the group velocities of the two eigenmodes do not coincide, *i.e.* the two curves do not cross with the same slope, and each group velocity matches well with the derivative of one approximated dispersion curve in the sense that the magnitude of the difference does not exceed an error tolerance of $\epsilon_{\text{tol}}^{\text{msb}}$, we take this as evidence that the two dispersion curves cross.

On the other hand, if the two group velocities are very close, *i.e.* the two dispersion curves have approximately the same slope at k_0 , we also have to compute higher derivatives of the dispersion curves at k_0 using the formula (3.5) and compare them with the corresponding derivatives of the approximated dispersion curves (5.1). In fact we have to compute derivatives of order n , if the derivatives of the two dispersion curves coincide up to order $n-1$. If for all m , with $1 \leq m \leq n$, the derivatives of order m of the two dispersion curves coincide with one of the derivatives of order m of the two approximated dispersion curves, *i.e.* the magnitude of the difference does not exceed an error tolerance of $\epsilon_{\text{tol}}^{\text{msb}}$, we shall assume that the two dispersion curves cross. Otherwise, we refine our approximations by additionally applying the adaptive scheme to the dispersion curves around k_0 , taking k_0 as start value and stopping the scheme if a value of k is reached for which we already solved the eigenvalue problem (2.2).

If we compare derivatives up to order n we shall denote this test as n -th order mini-stop band check. If $n=1$, we simply call it mini-stop band check.

Note that the mini-stop band check can also be understood as a validation test for crossings, in particular in the case when the two curves cross and have the same slope at the crossing. To this end, we also perform the mini-stop band check if the curves come

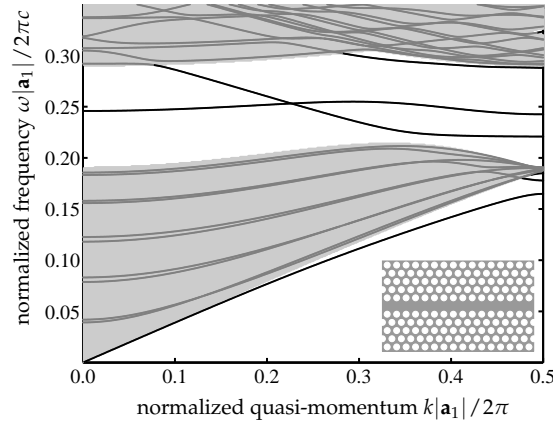


Figure 8: Band structure (black lines) of the TE mode in a hexagonal W1 PhC waveguide. The holes of relative radius 0.31 have permittivity $\varepsilon = 1$ and are surrounded by dielectric material of permittivity $\varepsilon = 11.4$. The computation was performed using the supercell method with five periodicity cells on top and bottom. The frequencies at which propagating PhC modes exist are shaded in grey while blank areas represent the band gaps.

very close (but do not cross). For those points it is necessary to perform at least a second order mini-stop band check, *i.e.* it is necessary to consider not only the group velocity but (at least) also the second derivative.

6 Numerical experiments

In this section we want to test the proposed adaptive scheme and show numerical results. We start with the TE mode band structure of a PhC W1 waveguide and of a perturbed W1 waveguide, before we will return to the TM mode band structure of Example 2.1.

Band structure of a PhC W1 waveguide Let us consider a PhC W1 waveguide with hexagonal lattice and holes of relative radius $r/|\mathbf{a}_1| = 0.31$ and permittivity $\varepsilon = 1$ in a dielectric medium of permittivity $\varepsilon = 11.4$ as in [35]. We fix the number of periodicity cells that are included in the supercell on top and bottom of the guide to be $n_{sc} = 5$, and study the TE mode of this configuration. We choose the periodicity cell to be the parallelogram around a hole. This means that our supercell comprises exactly ten holes, five on top of the guide and five below the guide. Note that this also implies that \mathbf{a}_1 and \mathbf{a}_2 , see Fig. 1(b), are not perpendicular but $\mathbf{a}_1 = |\mathbf{a}_1|(1,0)^T$ and $\mathbf{a}_2 = (2n_{sc} + 1)|\mathbf{a}_1|(0.5, \sqrt{0.75})^T$. Fig. 8 shows an overview of the band structure where the dispersion curves are represented by black lines and frequencies with propagating PhC modes are shaded in grey.

Let us now present the results of the adaptive scheme introduced above. We choose a desired error tolerance of $\varepsilon_{tol}^{step} = 10^{-4}$ to compute the acceptable step sizes, set the order of the expansion to $n = 10$, the start value of the iteration to $k^{(0)} = \pi/(2|\mathbf{a}_1|)$, and ap-

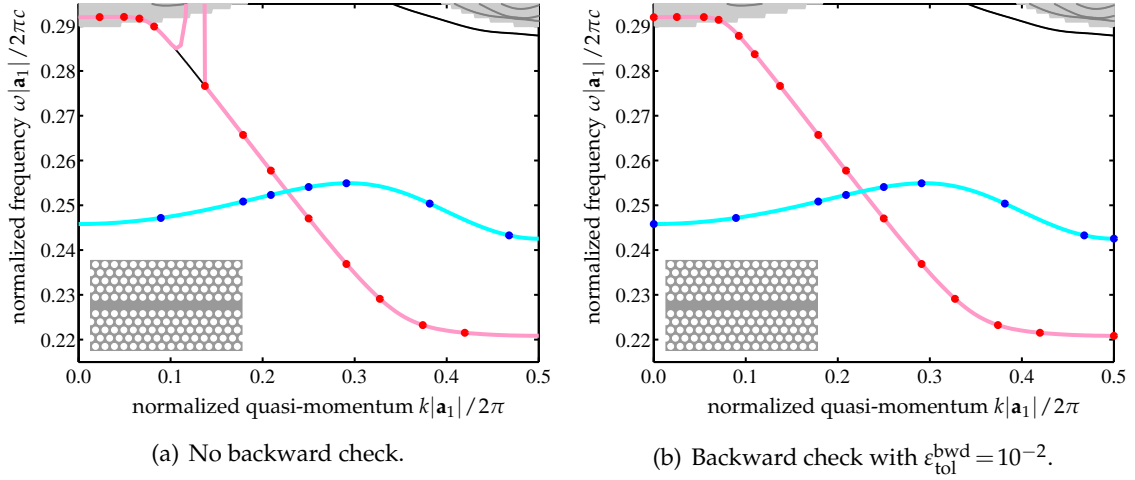


Figure 9: Adaptive Taylor scheme of order $n = 10$ applied to dispersion curves of the hexagonal W1 PhC waveguide. The error tolerance of the step size computation is $\epsilon_{\text{tol}}^{\text{step}} = 10^{-4}$ and the start value of the iteration is set to $k^{(0)} = \pi/(2|\mathbf{a}_1|)$.

ply the adaptive scheme without any additional checks to the two guided modes in the frequency interval $[0.2 \cdot 2\pi c/|\mathbf{a}_1|, 0.3 \cdot 2\pi c/|\mathbf{a}_1|]$ of the TE mode in the hexagonal W1 PhC waveguide as shown in Fig. 8.

The results can be seen in Fig. 9(a) where the dots indicate the location of the values of k for which the dispersion relation $\omega(k)$ and its derivatives $\omega'(k), \omega^{(2)}(k), \dots, \omega^{(10)}(k)$ were computed. The lines connecting the dots result from the post-processing, where we chose the weighted Taylor expansion (5.1). Note that the red dispersion curve leaves the band gap at $k \approx 0.1 \cdot 2\pi/|\mathbf{a}_1|$ and enters the frequency domain for which propagating PhC modes exist. Nevertheless, we can continue following this curve towards $k=0$ since each point on this curve still represents an eigenmode of the supercell method. However, we need to have in mind, that these supercell eigenmodes are spurious and that this part of the dispersion curve has no physical meaning. Most noticeable is the numerical artifact of the red line between $k \approx 0.08 \cdot 2\pi/|\mathbf{a}_1|$ and $k \approx 0.14 \cdot 2\pi/|\mathbf{a}_1|$. Recall, that we chose $k^{(0)} = \pi/(2|\mathbf{a}_1|)$ and hence, we followed the dispersion curve in this part from right to left. For the computation of the acceptable step size the derivatives at $k \approx 0.14 \cdot 2\pi/|\mathbf{a}_1|$ are relevant. But obviously, the derivatives at $k \approx 0.08 \cdot 2\pi/|\mathbf{a}_1|$ are significantly larger in magnitude than at $k \approx 0.14 \cdot 2\pi/|\mathbf{a}_1|$ yielding a smaller step size in the following step (distance to next red dot) and hence, explain the numerical error in the post-processing. This numerical artifact can be eliminated when performing the backward check. The results are presented in Fig. 9(b) where we chose an error tolerance of $\epsilon_{\text{tol}}^{\text{bwd}} = 10^{-2}$ for the backward check.

Clearly, the computational costs of the adaptive scheme including backward check are smaller than the costs of the standard procedure to solve the eigenvalue problem (2.2)

for an equidistant sample of quasi-momenta k , if one aims to get the same accuracy as the adaptive scheme. In the post-processing of the adaptive Taylor expansions in Fig. 9 we chose an equidistant sample of 100 values of the quasi-momentum k for which we computed the weighted Taylor expansion and from which we draw the solid red and blue curves. This shall deal as a reference for the desired accuracy. That means the standard procedure to calculate the band structure is to solve 100 eigenvalue problems (2.2). On the other hand, the adaptive scheme including backward check for the unperturbed waveguide accounts for 25 eigenvalue problems (2.2) and the computation of the frequency derivatives (3.5) of 24 modes, where we solve the eigenvalue problem (2.2) at $k=0$, $k=\pi/|\mathbf{a}_1|$ and $k=k^{(0)}$ for two eigenvalues in order to save time. Four eigenmodes of these 25 eigenvalue computations are rejected due to the backward check which explains that the number of nodes for which we compute the frequency derivatives (3.5) is smaller than the number of eigenvalue problems (2.2) to be solved. Considering that the computational costs of solving (3.5) for the frequency derivatives is significantly smaller than solving the eigenvalue problem (2.2), we can expect clearly smaller computational costs of the adaptive scheme compared to the standard procedure. Note that the computational advantage of the adaptive scheme especially becomes obvious in the case of a rather simple dispersion curve, *e.g.* the blue curve in Fig. 9. In fact, only a very small number of eigenvalue problems and corresponding source problems have to be computed in order to figure out the dispersion curve's slope correctly.

Mini-stop band of a perturbed PhC W1 waveguide Now we want to test the proposed mini-stop band check. Applied to the numerical example above, a W1 waveguide with hexagonal lattice which is symmetric with respect to the line defect, we find that a refinement is not necessary since the approximated slopes and computed group velocities at the projected crossing match well, which is in line with the theory [31] that says that modes with even parity (red dispersion curve) and modes with odd parity (blue dispersion curve) have to cross and do not form a mini-stop band. Therefore, we shall apply our mini-stop band check to a perturbed configuration. We shift the upper PhC by as little as $10^{-4}|\mathbf{a}_1|$ to the left. This breaks the symmetry and we can expect that the crossing of the two guided modes becomes an anti-crossing.

In Fig. 10 we show the results of the adaptive Taylor scheme including backward check with tolerance $\varepsilon_{\text{tol}}^{\text{bw}} = 10^{-2}$ applied to the perturbed W1 waveguide of hexagonal lattice. The results are very similar to the results of the unperturbed waveguide in Fig. 9(b). In particular, the approximated dispersion curves cross in Fig. 10 which we know is not true. Thus, a mini-stop band check as introduced above needs to be performed in order to identify the anti-crossing correctly. The two approximated dispersion curves in Fig. 10 cross at $k_0 \approx 0.227 \cdot 2\pi/|\mathbf{a}_1|$ and their slopes are approximately $-0.261c$ (red curve) and $0.044c$ (blue curve). But when solving the eigenvalue problem (2.2) at k_0 we find two eigenmodes which have both negative group velocity, and hence — using a tolerance $\varepsilon_{\text{tol}}^{\text{msb}} = 10^{-2}$ for the mini-stop band check — a refinement at k_0 is necessary. The result can be seen in Fig. 11 where we also show a detailed view of the mini-stop band.

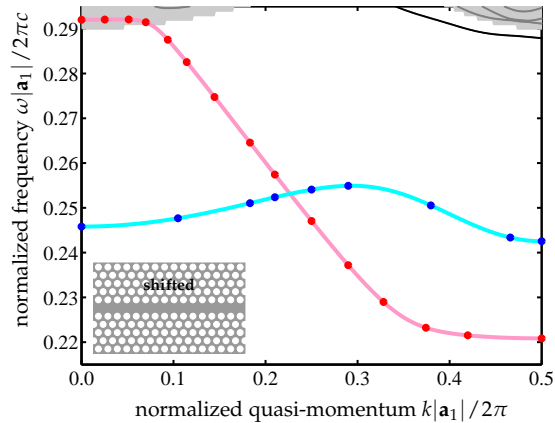


Figure 10: Adaptive Taylor scheme of order $n = 10$ with backward check of tolerance $\epsilon_{\text{tol}}^{\text{bwd}} = 10^{-2}$ applied to dispersion curves of the perturbed W1 PhC waveguide of hexagonal lattice (upper PhC shifted by $10^{-4}|\mathbf{a}_1|$ to the left). The error tolerance of the step size computation is $\epsilon_{\text{tol}}^{\text{step}} = 10^{-4}$ and the start value of the iteration is set to $k^{(0)} = \pi/(2|\mathbf{a}_1|)$.

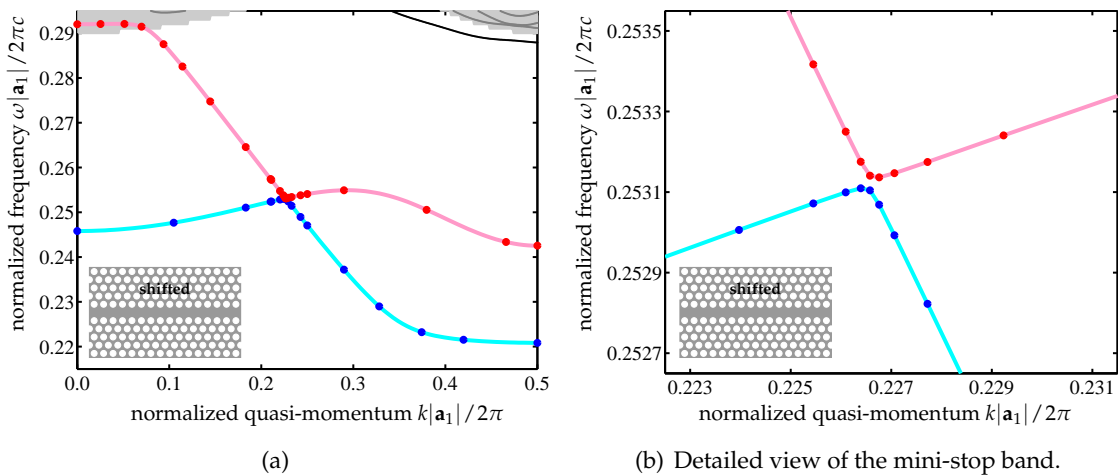


Figure 11: Adaptive Taylor scheme of order $n = 10$ with backward check of tolerance $\epsilon_{\text{tol}}^{\text{bwd}} = 10^{-2}$ and first order mini-stop band check of tolerance $\epsilon_{\text{tol}}^{\text{msb}} = 10^{-2}$ applied to dispersion curves of the perturbed W1 PhC waveguide with hexagonal lattice (upper PhC shifted by $10^{-4}|\mathbf{a}_1|$ to the left). The error tolerance of the step size computation is $\epsilon_{\text{tol}}^{\text{step}} = 10^{-4}$ and the start value of the iteration is set to $k^{(0)} = \pi/(2|\mathbf{a}_1|)$.

The computational advantage of the proposed adaptive Taylor expansion compared to the standard procedure even increases when trying to identify mini-stop bands. The adaptive scheme including backward check but without mini-stop band check, as presented in Fig. 10, accounts for 25 eigenvalue problems (2.2) and the computation of the

frequency derivatives (3.5) for 24 modes. When additionally performing the mini-stop band check and refining near the anti-crossing, as done in Fig. 11, we have another 13 eigenvalue problems (2.2) and a total of 26 frequency derivatives (3.5) to solve. We save time by simultaneously refining both dispersion curves together with the same step size and solving (3.5) for two eigenvalues, while computing the frequency derivatives (3.5) of all 26 computed eigenmodes. This makes a total of 38 eigenvalue problems (2.2) and 50 frequency derivatives (3.5), that we have to solve in order to approximate the two dispersion curves of the perturbed waveguide as presented in Fig. 11. Using the standard procedure to compute the band structure would clearly comprise the solution of more eigenvalue problems (2.2) since a very dense grid of values of the quasi-momentum k is needed in order to resolve the mini-stop band as accurate as in Fig. 11(b).

Dispersion curves intersecting with identical group velocity Now let us return to Example 2.1. We want to study the behaviour of our numerical scheme when two dispersion curves intersect at a point but do not cross. This is the case for the second and third dispersion curves at $k=0$, as can be seen from the band structure in Fig. 3. Due to symmetry at $k=0$, we restricted our computations so far to the reduced Brillouin zone $\widehat{B}=[0, \pi/|\mathbf{a}_1|]$. Now let us consider the complete Brillouin zone $B=[-\pi/|\mathbf{a}_1|, \pi/|\mathbf{a}_1|]$ having in mind that the band structure is symmetric with respect to the frequency axis at $k=0$. That means we know in advance that the two dispersion curves, that have a common eigenvalue at $k=0$, do not cross but touch only. Let us now study if our adaptive scheme can construct this band structure correctly. We choose the start point $k^{(0)}=0.01 \cdot 2\pi/|\mathbf{a}_1|$. Recall that we cannot choose $k^{(0)}=0$, the centre of the Brillouin zone B , since the second and third dispersion curves intersect at this point and hence, the multiplicity of the eigenvalue at $k=0$ is two, which implies that the group velocity formula (3.2), as well as the formula for higher derivatives, Eq. (3.5), is not well-defined without knowledge about the eigenmodes in the vicinity of $k=0$, as we elaborated in Remark 3.1.

We start by setting the order of the Taylor expansion to $n=1$. The step size tolerance is chosen to be $\varepsilon_{\text{tol}}^{\text{step}}=10^{-4}$ and we employ the backward check with tolerance $\varepsilon_{\text{tol}}^{\text{bwd}}=10^{-2}$ but do not use the mini-stop band check. Fig. 12(a) shows the numerical result for this configuration. We can see that the second dispersion curve (blue) is computed incorrectly, since from $k=0$ to the left it follows the third dispersion curve (red). When choosing a smaller backward check tolerance, as done in Fig. 12(b), where we set $\varepsilon_{\text{tol}}^{\text{bwd}}=10^{-4}$, we do not resolve this problem. In fact, both tolerance parameters, $\varepsilon_{\text{tol}}^{\text{bwd}}$ as well as the step size tolerance $\varepsilon_{\text{tol}}^{\text{step}}$, cannot be chosen small enough since an expansion of first order cannot account for the curvature of the dispersion curve. This explains that an expansion of first order is in general not a good choice no matter how small the tolerance parameters are chosen.

Now we increase the order of the expansion to $n=2$ and choose again $\varepsilon_{\text{tol}}^{\text{bwd}}=10^{-2}$. Fig. 13(a) shows that the two dispersion curves are computed correctly. However, using an expansion of order $n=2$ does not always resolve the problem as Fig. 13(b) shows,

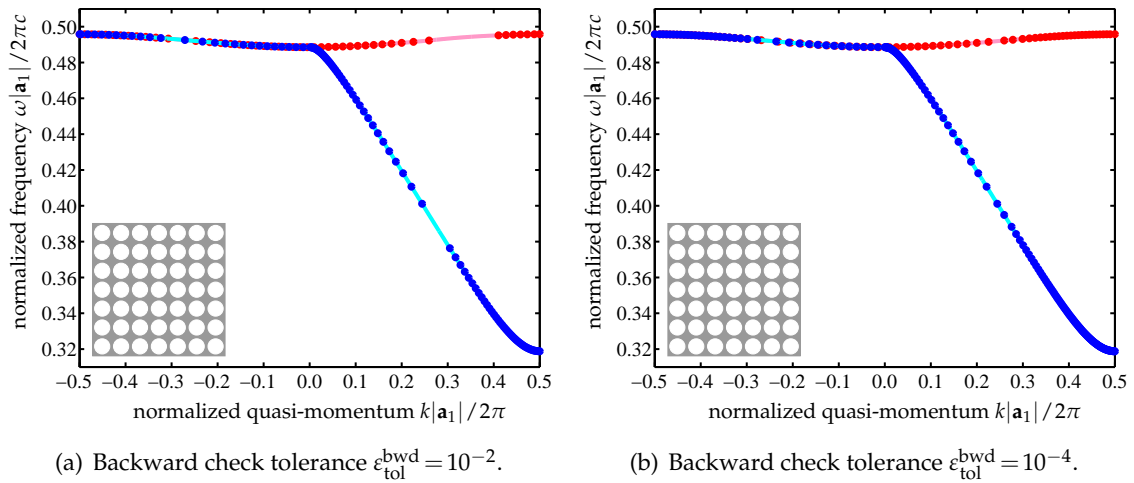


Figure 12: Adaptive Taylor scheme of order $n=1$ with backward check applied to the second and third dispersion curves of Example 2.1. The start value of the scheme is set to $k^{(0)} = 0.01 \cdot 2\pi / |\mathbf{a}_1|$.

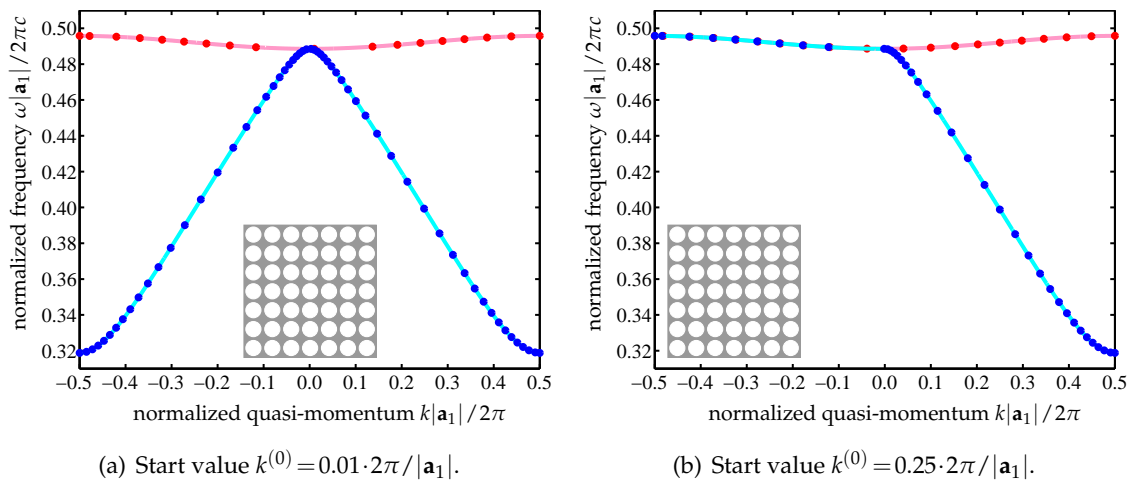


Figure 13: Adaptive Taylor scheme of order $n=2$ with backward check of tolerance $\epsilon_{\text{tol}}^{\text{bwd}} = 10^{-2}$ applied to the second and third dispersion curves of Example 2.1.

where we set the start value of the scheme to $k^{(0)} = 0.25 \cdot 2\pi / |\mathbf{a}_1|$. It turns out that we were only lucky by previously setting the start value to $k^{(0)} = 0.01 \cdot 2\pi / |\mathbf{a}_1|$, where the second derivative is large enough in magnitude to account for the correct slope of the second dispersion curve. In the case presented in Fig. 13(b), however, the tolerance parameters $\epsilon_{\text{tol}}^{\text{step}}$ and $\epsilon_{\text{tol}}^{\text{bwd}}$ are chosen too large so that the adaptive scheme does not place a Taylor node close enough to $k = 0$ and hence, the magnitude of the second derivative at the smallest positive node is too small to account for the correct curvature at $k = 0$.

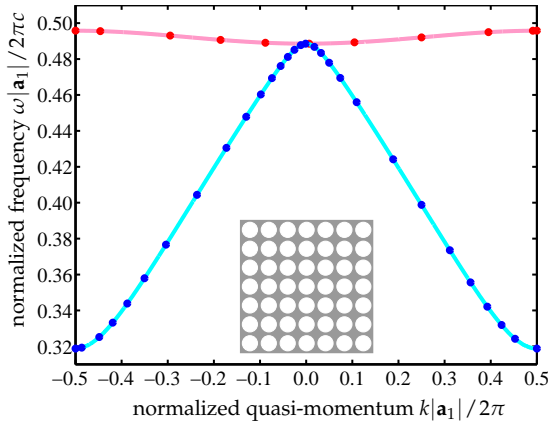


Figure 14: Adaptive Taylor scheme of order $n=3$ with backward check of tolerance $\epsilon_{\text{tol}}^{\text{bwd}} = 10^{-2}$ applied to the second and third dispersion curves of Example 2.1. The start value of the scheme is set to $k^{(0)} = 0.25 \cdot 2\pi / |\mathbf{a}_1|$.

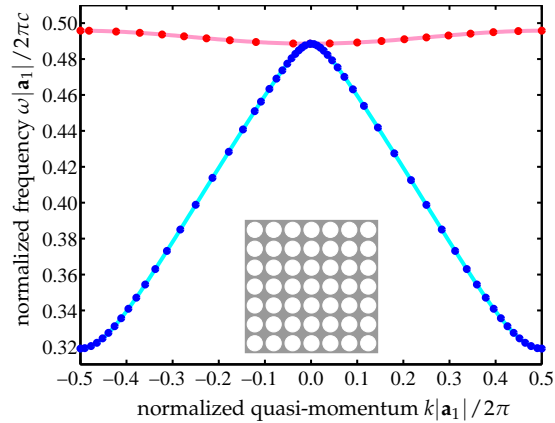


Figure 15: Adaptive Taylor scheme of order $n=2$ with backward check of tolerance $\epsilon_{\text{tol}}^{\text{bwd}} = 10^{-2}$ and second order mini-stop band check of tolerance $\epsilon_{\text{tol}}^{\text{msb}} = 10^{-2}$ applied to the second and third dispersion curves of Example 2.1. The start value of the scheme is set to $k^{(0)} = 0.25 \cdot 2\pi / |\mathbf{a}_1|$.

Choosing a smaller backward check tolerance may help to resolve this problem. When selecting a higher order we can also resolve this problem, as shown in Fig. 14, where we set the order to $n=3$, keeping the start value at $k^{(0)} = 0.25 \cdot 2\pi / |\mathbf{a}_1|$ and leaving the backward check tolerance unchanged.

Alternatively, we can do a second order mini-stop band check in order to resolve this problem even if we keep $n=2$ and $\epsilon_{\text{tol}}^{\text{bwd}} = 10^{-2}$. The two approximated dispersion curves in Fig. 13(b) come very close near $k=0$. In fact, we observe that the two approximated curves cross at $k_0 \approx 0.02 \cdot 2\pi / |\mathbf{a}_1|$. At k_0 we solve the eigenvalue problem and compare the first and second derivatives of the dispersion relation with the slopes and curvatures of the approximated curves. It turns out that the second derivatives do not match well with the curvatures of the approximated curves. We refine the approximation as described in the section on the mini-stop band check and find that the left branch of the refined blue curve does not fit to the left branch shown in Fig. 13(b), so that a full computation of the adaptive approximation in the interval $[-\pi / |\mathbf{a}_1|, k_0]$ is necessary. This yields the band structure presented in Fig. 15, which shows that the adaptive scheme with second order mini-stop band check produces appropriate approximations of two dispersion curves intersecting with the same slope, even if the order is as low as $n=2$.

To summarize, we note that an expansion of order two or larger is needed to correctly identify the behaviour of two curves, that intersect with the same slope. An expansion of order larger than two is preferable in order to decrease the influence of the start value on the approximation. A second order mini-stop band check can be employed to resolve the intersection correctly.

7 Conclusions

We presented the derivation and computation of the group velocity and higher derivatives of the dispersion relation of PhC modes and guided modes in PhC waveguides. For the computation of guided modes in PhC waveguides we employed the supercell and the DtN approach. These derivatives are used in a Taylor expansion of the dispersion curves which allows for an efficient calculation of the PhC band structure. We proposed an adaptive scheme for the efficient and reliable selection of the nodes, at which the eigenvalue problem is solved and the derivatives are computed. We showed that with our approach it is possible to verify crossings of dispersion curves, as well as to identify mini-stop bands even if they are very narrow.

The computational costs are smaller compared to the standard procedure of solving the eigenvalue problem for a fine, uniform grid of values of the quasi-momentum, for both, rather simple dispersion curves, whose derivatives have small magnitudes, and complicated dispersion curves, that form a mini-stop band for example.

A Proof of the piecewise differentiability of the eigenmodes

We shall assume here and in the sequel that the eigenvalue multiplicity of all dispersion curves is one almost everywhere in B .

Let $k_0 \in B$ and let $\omega_m^2(k_0)$ be an eigenvalue of (2.2) with geometric multiplicity one. Due to the above assumption there exists $h_0 > 0$ such that for all $h \in]-h_0, h_0[$ the eigenvalue $\omega_m^2(k_0+h)$ of (2.2) has geometric multiplicity one. The eigenmodes $u_m(\cdot; k_0+h)$ corresponding to the eigenvalues $\omega_m^2(k_0+h)$ are unique up to a complex-valued multiplicative factor. Continuity and differentiability of these eigenmodes with respect to k at $k=k_0$ is hence subject to a complex scaling of $u_m(\cdot; k_0+h)$ for all $h \in]-h_0, h_0[$.

Lemma A.1. *Let $u_m(\cdot; k_0+h)$, with $h \in]-h_0, h_0[$, be an arbitrary eigenmode of (2.2) at $k = k_0+h$ with $H^1(C)$ -norm 1 that corresponds to the eigenvalue $\omega_m^2(k_0+h)$. Then, in the limit $h \rightarrow 0$, $u_m(\cdot; k_0+h)$ is an eigenmode of (2.2) at $k=k_0$ corresponding to the eigenvalue $\omega_m^2(k_0)$ and $u_m(\cdot; k_0+h) \rightarrow cu_m(\cdot; k_0)$ in $H_{\text{per}}^1(C)$ for some $c \in \mathbb{C}$ with $|c|=1$.*

Proof. We know that $u_m(\cdot; k_0)$ satisfies

$$\int_C \alpha(\nabla + ik_0 \mathbf{a}_1) u_m(\cdot; k_0) \cdot (\nabla - ik_0 \mathbf{a}_1) \bar{v} - \omega_m^2(k_0) \beta u_m(\cdot; k_0) \bar{v} \, dx = 0$$

for all $v \in H_{\text{per}}^1(C)$ and $u_m(\cdot; k_0+h)$ satisfies

$$\int_C \alpha(\nabla + i(k_0+h) \mathbf{a}_1) u_m(\cdot; k_0+h) \cdot (\nabla - i(k_0+h) \mathbf{a}_1) \bar{v} - \omega_m^2(k_0+h) \beta u_m(\cdot; k_0+h) \bar{v} \, dx = 0$$

for all $v \in H_{\text{per}}^1(C)$. Consequently, the function $e_m(\cdot; h) := u_m(\cdot; k_0+h) - u_m(\cdot; k_0)$ satisfies

$$\int_C \alpha(\nabla + ik_0 \mathbf{a}_1) e_m(\cdot; h) \cdot (\nabla - ik_0 \mathbf{a}_1) \bar{v} - \omega_m^2(k_0) \beta e_m(\cdot; h) \bar{v} \, dx = g_{m,h}(v)$$

for all $v \in H^1_{\text{per}}(C)$ with the linear form

$$\begin{aligned}
 g_{m,h}(v) &= (\omega_m^2(k_0+h) - \omega_m^2(k_0)) \int_C \beta u_m(k_0+h) \bar{v} \, dx \\
 &\quad + h \int_C \alpha (\nabla + ik_0 \mathbf{a}_1) u_m(k_0+h) \cdot i \mathbf{a}_1 \bar{v} - \alpha i \mathbf{a}_1 u_m(k_0+h) \cdot (\nabla - ik_0 \mathbf{a}_1) \bar{v} \, dx \\
 &\quad - h^2 \int_C \alpha |\mathbf{a}_1|^2 u_m(k_0+h) \bar{v} \, dx.
 \end{aligned}$$

Since ω_m^2 is continuous at $k = k_0$, we know that $g_{m,h}(v) \rightarrow 0$ as $h \rightarrow 0$. Hence, in the limit $h \rightarrow 0$ the function $e_m(\cdot;h)$ is either zero or it is an eigenmode of (2.2) at $k = k_0$ with corresponding eigenvalue $\omega_m^2(k_0)$. Since the geometric multiplicity of $\omega_m^2(k_0)$ is one, we can conclude that in both cases $\lim_{h \rightarrow 0} e_m(\cdot;h) = \tilde{c} u_m(\cdot; k_0)$ with some complex number $\tilde{c} \in \mathbb{C}$. This implies that $\lim_{h \rightarrow 0} u_m(\cdot; k_0+h) = c u_m(\cdot; k_0)$, with $c = \tilde{c} + 1$. Now we use the fact that $\|u_m(\cdot; k_0+h)\|_{H^1(C)} = 1$ for all $h \in]h_0, h_0[$ and hence, — taking the norm of the previous equation — we can conclude that $|c| = 1$, which finishes the proof. \square

Now let us — in addition to the norm — also fix the phase of the eigenmode. To this end, we define $w := u_m(\cdot; k_0)$ as an arbitrary but fixed eigenmode of (2.2) at $k = k_0$ with $H^1(C)$ -norm 1. Then we introduce the following problem: find $\tilde{u}_m(\cdot; k) \in H^1_{\text{per}}(C)$, $k = k_0 + h$, and the Lagrangian multiplier $\lambda_{\tilde{u}_m}(k) \in \mathbb{C}$ that satisfy

$$\int_C \alpha (\nabla + i k \mathbf{a}_1) \tilde{u}_m(k) \cdot (\nabla - i k \mathbf{a}_1) \bar{v} - \omega_m^2(k) \beta \tilde{u}_m(k) \bar{v} \, dx + \lambda_{\tilde{u}_m}(k) \langle w, v \rangle_{H^1(C)} = 0, \tag{A.1a}$$

$$\langle \tilde{u}_m(k), w \rangle_{H^1(C)} = 1, \tag{A.1b}$$

for all $v \in H^1_{\text{per}}(C)$ where $\langle \cdot, \cdot \rangle_{H^1(C)}$ denotes the usual $H^1(C)$ -inner product, i. e. $\langle u, v \rangle_{H^1(C)} = \int_C \nabla u \cdot \nabla \bar{v} + u \bar{v} \, dx$.

Lemma A.2. *If k is sufficiently close to k_0 , the problem (A.1) has a unique solution.*

Proof. First let us prove existence. Let $u_m(\cdot; k)$ denote an arbitrary eigenmode of (2.2) with $H^1(C)$ -norm 1 associated to $\omega_m^2(k)$, and let $c(h) = \langle u_m(k), w \rangle_{H^1(C)}$. From Lemma A.1 we know that $u_m(\cdot; k) \rightarrow c w$ as $h \rightarrow 0$ for some $c \in \mathbb{C}$ with $|c| = 1$. This implies that $c(h) \rightarrow c$ as $h \rightarrow 0$ and hence, $c(h) \neq 0$ if k is sufficiently close to k_0 . Then, $\tilde{u}_m(\cdot; k) = \frac{1}{c(h)} u_m(\cdot; k)$ solves (A.1) with the Lagrangian multiplier $\lambda_{\tilde{u}_m}(k) = 0$.

Now let us prove uniqueness. To this end, we assume that — apart from the eigenmode solution $(\tilde{u}_{m,1}(\cdot; k), \lambda_{\tilde{u}_{m,1}}(k)) = (\tilde{u}_m(\cdot; k), 0) \in H^1_{\text{per}}(C) \times \mathbb{C}$ — there exists another solution $(\tilde{u}_{m,2}(\cdot; k), \lambda_{\tilde{u}_{m,2}}(k)) \in H^1_{\text{per}}(C) \times \mathbb{C}$ with $\tilde{u}_{m,2}(\cdot; k) \not\equiv \tilde{u}_{m,1}(\cdot; k)$ or $\lambda_{\tilde{u}_{m,2}}(k) \neq \lambda_{\tilde{u}_{m,1}}(k) = 0$. Since $(\tilde{u}_{m,2}(\cdot; k), \lambda_{\tilde{u}_{m,2}}(k))$ is a solution of (A.1), we can write

$$\begin{aligned}
 \int_C \alpha (\nabla + i k \mathbf{a}_1) \tilde{u}_{m,2}(k) \cdot (\nabla - i k \mathbf{a}_1) \bar{v} - \omega_m^2(k) \beta \tilde{u}_{m,2}(k) \bar{v} \, dx + \lambda_{\tilde{u}_{m,2}}(k) \langle w, v \rangle_{H^1(C)} &= 0, \\
 \langle \tilde{u}_{m,2}(k), w \rangle_{H^1(C)} &= 1,
 \end{aligned}$$

for all $v \in H_{\text{per}}^1(C)$. Now we test the first equation with $v = \tilde{u}_m(\cdot; k)$. Since this is an eigenmode of (2.2) and it satisfies the constraint condition (A.1b), we obtain $\lambda_{\tilde{u}_m,2}(k) = 0$. However, this implies that $\tilde{u}_m(\cdot; k)$ is an eigenmode of (2.2). But from the constraint condition (A.1b) and the assumption that the two solutions are not identical, it follows that $\tilde{u}_m(\cdot; k) \neq c\tilde{u}_m,1(\cdot; k)$ with some $c \in \mathbb{C}$. Hence, $\tilde{u}_m(\cdot; k)$ is an eigenmode of (2.2) that is linear independent of the eigenmode $\tilde{u}_m,1(\cdot; k)$, which is a contradiction to our assumption that the multiplicity of the eigenvalue problem (2.2) is one at $k \in]k_0 - h_0, k_0 + h_0[$. \square

Now we are able to state the following result.

Corollary A.1. *The unique solution $\tilde{u}_m(\cdot; k)$ of (A.1) is an eigenmode of (2.2) with associated eigenvalue $\omega_m^2(k)$.*

Finally, we can prove continuity of $\tilde{u}_m(\cdot; k)$ at $k = k_0$.

Lemma A.3. *For all $m \in \mathbb{N}$, the eigenmode $\tilde{u}_m(\cdot; k)$ that solves (A.1) is continuous at $k = k_0$.*

Proof. Let $\tilde{e}_m(\cdot; h) := \tilde{u}_m(\cdot; k_0 + h) - \tilde{u}_m(\cdot; k_0)$, $h \in]-h_0, h_0[$. We introduce the Lagrangian multiplier $\lambda_{\tilde{e}_m}(h) = \lambda_{\tilde{u}_m}(k_0 + h) - \lambda_{\tilde{u}_m}(k_0)$ and hence, the function $\tilde{e}_m(h)$ satisfies

$$\begin{aligned} & \int_C \alpha(\nabla + ik_0 \mathbf{a}_1) \tilde{e}_m(h) \cdot (\nabla - ik_0 \mathbf{a}_1) \bar{v} - \omega_m^2(k_0) \beta \tilde{e}_m(h) \bar{v} \, dx + \lambda_{\tilde{e}_m}(h) \langle w, v \rangle_{H^1(C)} \\ &= (\omega_m^2(k_0 + h) - \omega_m^2(k_0)) \int_C \beta \tilde{u}_m(k_0 + h) \bar{v} \, dx \\ & \quad + h \int_C \alpha(\nabla + ik_0 \mathbf{a}_1) \tilde{u}_m(k_0 + h) \cdot i \mathbf{a}_1 \bar{v} - \alpha i \mathbf{a}_1 \tilde{u}_m(k_0 + h) \cdot (\nabla - ik_0 \mathbf{a}_1) \bar{v} \, dx \\ & \quad - h^2 \int_C \alpha |\mathbf{a}_1|^2 \tilde{u}_m(k_0 + h) \bar{v} \, dx, \end{aligned} \tag{A.2a}$$

$$\langle \tilde{e}_m(h), w \rangle_{H^1(C)} = \langle \tilde{u}_m(k_0 + h) - \tilde{u}_m(k_0), w \rangle_{H^1(C)}, \tag{A.2b}$$

for all $v \in H_{\text{per}}^1(C)$. The term on the right hand side of Eq. (A.2b) vanishes since both functions, $\tilde{u}_m(k_0 + h)$ and $\tilde{u}_m(k_0)$, satisfy Eq. (A.1a). Since $k \mapsto \omega_m(k)$ is continuous at $k = k_0$ we conclude that the right hand side of Eq. (A.2a) tends to zero as $h \rightarrow 0$, and hence, — considering that the problem (A.2) is well-posed — we have $\tilde{e}_m(h) \rightarrow 0$ in $H_{\text{per}}^1(C)$ as $h \rightarrow 0$, which finishes the proof. \square

In order to prove that $\tilde{u}_m(\cdot; k)$ is differentiable at $k = k_0$ we introduce a new mixed variational problem: find $\tilde{u}'_m(k) \in H_{\text{per}}^1(C)$, $k = k_0 + h$, and the Lagrangian multiplier $\lambda_{\tilde{u}'_m}(k) \in \mathbb{C}$ that satisfy

$$\int_C \alpha(\nabla + ik \mathbf{a}_1) \tilde{u}'_m(k) \cdot (\nabla - ik \mathbf{a}_1) \bar{v} - \omega_m^2(k) \beta \tilde{u}'_m(k) \bar{v} \, dx + \lambda_{\tilde{u}'_m}(k) \langle w, v \rangle_{H^1(C)} = f_m^{(1)}(v; k), \tag{A.3a}$$

$$\langle \tilde{u}'_m(k), w \rangle_{H^1(C)} = 0 \tag{A.3b}$$

for all $v \in H^1_{\text{per}}(C)$ with the linear form

$$f_m^{(1)}(v;k) = \int_C \alpha(\nabla + ika_1)\tilde{u}_m(k) \cdot \mathbf{ia}_1 \bar{v} - \alpha \mathbf{ia}_1 \tilde{u}_m(k) \cdot (\nabla - ika_1)\bar{v} + (\omega_m^2(k))' \beta \tilde{u}_m(k) \bar{v} \, dx.$$

Using the same arguments as in the proof of Lemma A.2 we can conclude that (A.3) has a unique solution.

Remark A.1. Note that in the limit $h \rightarrow 0$, the problem (A.3) is equivalent to (3.3). In this context, it becomes clear that in the limit $h \rightarrow 0$ the Lagrangian multiplier $\lambda_{\tilde{u}'_m}(k)$ vanishes, see Remark 3.2. Since the compatibility condition of the mixed variational problem (A.3), *i. e.* taking the eigenmode $\tilde{u}_m(\cdot;k)$ as test function in (A.3a), yields $f_m^{(1)}(\tilde{u}_m(\cdot;k);k) = \lambda_{\tilde{u}'_m}(k)$, we can conclude that in the limit $h \rightarrow 0$ the compatibility condition of (A.3) yields the group velocity formula (3.2) with $u = \tilde{u}_m(\cdot;k)$.

Lemma A.4. For all $m \in \mathbb{N}$, the eigenmode $\tilde{u}_m(\cdot;k)$ that solves (A.1) is Fréchet differentiable with respect to k at $k = k_0$, and $\frac{d}{dk}\tilde{u}_m(\cdot;k_0) = \tilde{u}'_m(\cdot;k_0)$.

Proof. Let $\tilde{e}'_m(\cdot;h) := \frac{1}{h}(\tilde{u}_m(\cdot;k_0+h) - \tilde{u}_m(\cdot;k_0) - h\tilde{u}'_m(\cdot;k_0))$, $h \in]-h_0, h_0[$. Introducing the Lagrangian multiplier $\lambda_{\tilde{e}'_m}(h) = \frac{1}{h}(\lambda_{\tilde{u}_m}(k_0+h) - \lambda_{\tilde{u}_m}(k_0) - h\lambda_{\tilde{u}'_m}(k_0))$, the function $\tilde{e}'_m(h)$ satisfies

$$\begin{aligned} & \int_C \alpha(\nabla + ik_0 \mathbf{a}_1)\tilde{e}'_m(h) \cdot (\nabla - ik_0 \mathbf{a}_1)\bar{v} - \omega_m^2 \beta \tilde{e}'_m(h) \bar{v} \, dx + \lambda_{\tilde{e}'_m}(h) \langle w, v \rangle_{H^1(C)} \\ & = -f_m^{(1)}(v;k_0) + \tilde{f}_m(v;h), \end{aligned} \tag{A.4a}$$

$$\langle \tilde{e}'_m(h), w \rangle_{H^1(C)} = \frac{1}{h} \langle \tilde{u}_m(k_0+h) - \tilde{u}_m(k_0), w \rangle_{H^1(C)}, \tag{A.4b}$$

for all $v \in H^1_{\text{per}}(C)$ with the linear form

$$\begin{aligned} \tilde{f}_m(v;h) &= \int_C \alpha(\nabla + ik_0 \mathbf{a}_1)\tilde{u}_m(k_0+h) \cdot \mathbf{ia}_1 \bar{v} - \alpha \mathbf{ia}_1 \tilde{u}_m(k_0+h) \cdot (\nabla - ik_0 \mathbf{a}_1)\bar{v} \, dx \\ & \quad + \frac{\omega_m^2(k_0+h) - \omega_m^2(k_0)}{h} \int_C \beta \tilde{u}_m(k_0+h) \bar{v} \, dx - h \int_C \alpha |\mathbf{a}_1|^2 \tilde{u}_m(k_0+h) \bar{v} \, dx. \end{aligned}$$

The term on the right hand side of Eq. (A.4b) vanishes since both functions, $\tilde{u}_m(k_0+h)$ and $\tilde{u}_m(k_0)$, satisfy Eq. (A.1a). Finally, — using Proposition 2.1 and Lemma A.3 — we conclude that $\tilde{f}_m(\cdot;h) \rightarrow f_m^{(1)}(\cdot;k_0)$ as $h \rightarrow 0$, and hence, — considering that the problem (A.4) is well-posed — we have $\tilde{e}'_m(h) \rightarrow 0$ in $H^1_{\text{per}}(C)$ as $h \rightarrow 0$, which finishes the proof. \square

In order to extend the theory to higher orders we introduce $\tilde{u}_m^{(n)}(k) \in H^1_{\text{per}}(C)$, $n \in \mathbb{N}$, $k = k_0 + h$, as the unique solution of

$$\begin{aligned} & \int_C \alpha(\nabla + ika_1)\tilde{u}_m^{(n)}(k) \cdot (\nabla - ika_1)\bar{v} - \omega_m^2 \beta \tilde{u}_m^{(n)}(k) \bar{v} \, dx + \lambda_{\tilde{u}_m^{(n)}}(k) \langle w, v \rangle_{H^1(C)} = f_m^{(n)}(v;k), \\ & \langle \tilde{u}_m^{(n)}(k), w \rangle_{H^1(C)} = 0, \end{aligned}$$

for all $v \in H^1_{\text{per}}(C)$ with the Lagrangian multiplier $\lambda_{\tilde{u}_m^{(n)}} \in \mathbb{C}$ and the linear form

$$\begin{aligned}
 f_m^{(n)}(v; k) = & \sum_{p=0}^{n-1} \sum_{q=0}^{n-p} \frac{n!}{p!q!(n-p-q)!} \omega_m^{(n-p-q)}(k) \omega_m^{(q)}(k) \int_C \beta \tilde{u}_m^{(p)}(k) \bar{v} \, d\mathbf{x} \\
 & - i n |\mathbf{a}_1| \int_C \alpha \tilde{u}_m^{(n-1)}(k) (\partial_1 \bar{v}) - \alpha (\partial_1 \tilde{u}_m^{(n-1)}(k)) \bar{v} \, d\mathbf{x} \\
 & - 2nk |\mathbf{a}_1|^2 \int_C \alpha \tilde{u}_m^{(n-1)}(k) \bar{v} \, d\mathbf{x} - n(n-1) |\mathbf{a}_1|^2 \int_C \alpha \tilde{u}_m^{(n-2)}(k) \bar{v} \, d\mathbf{x}.
 \end{aligned}$$

Using the same arguments as in the proof of Lemma A.4 we conclude the following statement, which finishes the proof of the piecewise differentiability of the eigenmodes with respect to k up to any order.

Lemma A.5. *For all $m \in \mathbb{N}$, the eigenmode $\tilde{u}_m(\cdot; k)$ that solves (A.1) is Fréchet differentiable with respect to k at $k = k_0$ up to any order, and $\frac{d^n}{dk^n} \tilde{u}_m(\cdot; k_0) = \tilde{u}_m^{(n)}(\cdot; k_0)$.*

Now we are able to prove Proposition 2.2.

Proof of Proposition 2.2. Since w can be chosen to be any eigenmode of (2.2) at $k = k_0$, we showed that the eigenmodes of (2.2) associated to eigenvalues that have multiplicity one at $k = k_0$ are continuously differentiable with respect to k at $k = k_0$ up to any order, which is the desired result. \square

B Derivatives of dispersion curves for problems with Dirichlet-to-Neumann transparent boundary conditions

We will now present the formulas for the group velocity and all higher derivatives of the dispersion relation if we prescribe DtN transparent boundary conditions at the top and bottom boundaries Γ_T and Γ_B . Using DtN operators as shown in [22], the computational domain can be restricted to the defect cell C , *c.f.* Fig. 1(c), where the DtN operators $\Lambda^T(\omega, k) : u|_{\Gamma_T} \mapsto (\partial_2 u)|_{\Gamma_T}$ and $\Lambda^B(\omega, k) : u|_{\Gamma_B} \mapsto (-\partial_2 u)|_{\Gamma_B}$ are linear maps of the Dirichlet traces to the Neumann traces at the top and bottom boundaries Γ_T and Γ_B . The DtN operators can be computed by solving local cell problems in a unit cell of the PhC, and solving a quadratic matrix-valued equation. Also in [22], it was shown that the DtN operators are differentiable to any order with respect to ω and k inside the band gaps, *i. e.* $\frac{\partial^{m+n}}{\partial k^m \partial \omega^n} \Lambda^{T/B}(\omega, k)$ are well defined for any $m, n \in \mathbb{N}$ and can be computed using a set of local cell problems.

Since we do not prescribe periodic boundary conditions at Γ_T and Γ_B , we need a new Sobolev space for the weak formulation of the problem with DtN operators. To this end, let $H^1_{x_1\text{-per}}(C) \subset H^1(C)$ denote the space of $H^1(C)$ functions that are periodic in x_1 -direction. The corresponding variational formulation of the eigenvalue problem (2.2)

with DtN operators then reads: for any $k \in B$ find guided modes $u(\cdot; k) \in H^1_{x_1\text{-per}}(C)$ and corresponding eigenvalues $\omega^2(k) \in \mathbb{R}^+$ such that

$$\int_C \alpha(\nabla + ika_1)u \cdot (\nabla - ika_1)\bar{v} - \omega^2 \beta u \bar{v} \, dx - \int_{\Gamma_T} \alpha \Lambda^T(\omega, k) u \bar{v} \, ds(\mathbf{x}) - \int_{\Gamma_B} \alpha \Lambda^B(\omega, k) u \bar{v} \, ds(\mathbf{x}) = 0 \tag{B.1}$$

for all $v \in H^1_{x_1\text{-per}}(C)$.

According to Remark 2.1 the eigenvalues $\omega^2(k)$ can be ordered such that the dispersion curves $k \mapsto \omega_m(k)$ are continuously differentiable up to any order. We claim that a similar result holds true for the corresponding eigenmodes $u(k)$, see Remark 2.2, and hence, we can differentiate (B.1) with respect to k up to any order. The n -th derivative of Eq. (B.1) with respect to k splits into two terms and reads

$$\frac{d^n}{dk^n} \int_C \alpha(\nabla + ika_1)u \cdot (\nabla - ika_1)\bar{v} - \omega^2 \beta u \bar{v} \, dx - \frac{d^n}{dk^n} \left(\int_{\Gamma_T} \alpha \Lambda^T(\omega, k) u \bar{v} \, ds(\mathbf{x}) + \int_{\Gamma_B} \alpha \Lambda^B(\omega, k) u \bar{v} \, ds(\mathbf{x}) \right) = 0. \tag{B.2}$$

The first term is equivalent to the n -th derivative of Eq. (2.2) in Section 3, *i. e.*

$$\begin{aligned} & \frac{d^n}{dk^n} \int_C \alpha(\nabla + ika_1)u \cdot (\nabla - ika_1)\bar{v} - \omega^2 \beta u \bar{v} \, dx \\ &= \int_C \alpha(\nabla + ika_1) d_k^n u \cdot (\nabla - ika_1)\bar{v} - \omega^2 \beta d_k^n u \bar{v} \, dx - f_n(v), \end{aligned}$$

with f_n as given in Eq. (3.4). However, to the best of our knowledge, there does not exist a closed formula for the second term of Eq. (B.2), but it can be computed recursively. On the one hand, we have

$$\frac{d^n}{dk^n} \left(\Lambda^{T/B}(\omega(k), k) u \right) = \sum_{m=0}^n \binom{n}{m} \left(\frac{d^m}{dk^m} \Lambda^{T/B}(\omega(k), k) \right) d_k^{n-m} u,$$

and on the other hand we obtain the formula

$$\begin{aligned} \frac{d^n}{dk^n} \Lambda^{T/B}(\omega(k), k) &= \frac{d^{n-1}}{dk^{n-1}} \left(\omega' \Lambda_\omega^{T/B}(\omega(k), k) + \Lambda_k^{T/B}(\omega(k), k) \right) \\ &= \sum_{m=0}^{n-1} \binom{n-1}{m} \omega^{(1+m)} \frac{d^{n-m-1} \Lambda_\omega^{T/B}(\omega(k), k)}{dk^{n-m-1}} + \frac{d^{n-1} \Lambda_k^{T/B}(\omega(k), k)}{dk^{n-1}}, \tag{B.3} \end{aligned}$$

where we use the short notations $\Lambda_\omega^{T/B} = \frac{\partial \Lambda^{T/B}}{\partial \omega}$ and $\Lambda_k^{T/B} = \frac{\partial \Lambda^{T/B}}{\partial k}$. Eq. (B.3) can be used recursively to compute $\frac{d^n \Lambda^{T/B}}{dk^n}$ up to any order. To this end, we compute the partial derivatives $\frac{\partial^{(m+m')}\Lambda^{T/B}}{\partial \omega^m \partial k^{m'}}$ for all $m = 0, \dots, n$ and $m' = 0, \dots, n$, with $m + m' \leq n$. This can be done by

solving a set of local cell problems as described in [22]. Then we apply Eq. (B.3) recursively in order to evaluate total derivatives of partial derivatives until $\frac{d^n \Lambda^{T/B}}{dk^n}$ is expressed as a sum containing only partial derivatives.

From this we deduce that $d_k^n u \in H^1_{x_1\text{-per}}(C)$ satisfies

$$\int_C \alpha(\nabla + ika_1) d_k^n u \cdot (\nabla - ika_1) \bar{v} - \omega^2 \beta d_k^n u \bar{v} \, dx - \int_{\Gamma_T} \alpha \Lambda^T(\omega, k) d_k^n u \bar{v} \, ds(\mathbf{x}) - \int_{\Gamma_B} \alpha \Lambda^B(\omega, k) d_k^n u \bar{v} \, ds(\mathbf{x}) = f_n^{\text{DtN}}(v) \quad (\text{B.4})$$

for all $v \in H^1_{x_1\text{-per}}(C)$, with the linear form

$$f_n^{\text{DtN}}(v) = f_n(v) + \sum_{m=1}^n \binom{n}{m} \int_{\Gamma_T} \alpha \frac{d^m}{dk^m} \left(\Lambda^T(\omega(k), k) \right) d_k^{n-m} u \bar{v} \, ds(\mathbf{x}) + \sum_{m=1}^n \binom{n}{m} \int_{\Gamma_B} \alpha \frac{d^m}{dk^m} \left(\Lambda^B(\omega(k), k) \right) d_k^{n-m} u \bar{v} \, ds(\mathbf{x}),$$

where the terms $\frac{d^m}{dk^m} \left(\Lambda^{T/B}(\omega(k), k) \right)$ are determined recursively using Eq. (B.3). Testing Eq. (B.4) with $v = u$ yields $f_n^{\text{DtN}}(u) = 0$ from which we obtain the n -th derivative of the dispersion relation

$$\begin{aligned} \omega^{(n)} = & \left(2\omega \int_C \beta |u|^2 \, dx + \int_{\Gamma_T} \alpha \Lambda^T_\omega u \bar{u} \, ds(\mathbf{x}) + \int_{\Gamma_B} \alpha \Lambda^B_\omega u \bar{u} \, ds(\mathbf{x}) \right)^{-1} \\ & \times \left[n(n-1) |a_1|^2 \int_C \alpha d_k^{n-2} u \bar{u} \, dx + 2nk |a_1|^2 \int_C \alpha d_k^{n-1} u \bar{u} \, dx \right. \\ & + in |a_1| \int_C \alpha d_k^{n-1} u (\partial_1 \bar{u}) - \alpha (\partial_1 d_k^{n-1} u) \bar{u} \, dx \\ & - \sum_{p=1}^{n-1} \sum_{q=0}^{n-p} \frac{n!}{p!q!(n-p-q)!} \omega^{(n-p-q)} \omega^{(q)} \int_C \beta d_k^p u \bar{u} \, dx \\ & - \sum_{q=1}^{n-1} \frac{n!}{q!(n-q)!} \omega^{(n-q)} \omega^{(q)} \int_C \beta |u|^2 \, dx \\ & - \sum_{m=1}^{n-1} \binom{n}{m} \left(\int_{\Gamma_T} \alpha \frac{d^m \Lambda^T}{dk^m} d_k^{n-m} u \bar{u} \, ds(\mathbf{x}) + \int_{\Gamma_B} \alpha \frac{d^m \Lambda^B}{dk^m} d_k^{n-m} u \bar{u} \, ds(\mathbf{x}) \right) \\ & - \sum_{m=0}^{n-2} \binom{n-1}{m} \omega^{(1+m)} \left(\int_{\Gamma_T} \alpha \frac{d^{n-1-m} \Lambda^T_\omega}{dk^{n-m-1}} u \bar{u} \, ds(\mathbf{x}) + \int_{\Gamma_T} \alpha \frac{d^n \Lambda^T_k}{dk^n} u \bar{u} \, ds(\mathbf{x}) \right. \\ & \left. + \int_{\Gamma_B} \alpha \frac{d^{n-1-m} \Lambda^B_\omega}{dk^{n-m-1}} u \bar{u} \, ds(\mathbf{x}) + \int_{\Gamma_B} \alpha \frac{d^n \Lambda^B_k}{dk^n} u \bar{u} \, ds(\mathbf{x}) \right) \Big]. \quad (\text{B.5}) \end{aligned}$$

Analogously to the argumentation in Section 3, we note that Eq. (B.4) does not have a unique solution $d_k^n u \in H_{x_1\text{-per}}^1(C)$. However, by additionally requiring $H_{x_1\text{-per}}^1(C)$ -orthogonality to any eigenmode $u \in H_{x_1\text{-per}}^1(C)$ we can compute a particular solution $d_k^n u \in H_{x_1\text{-per}}^1(C)$ of Eq. (B.4). Again — for simplicity — let us assume that there exists only one linearly independent eigenmode $u(\cdot; k)$ corresponding to the eigenvalue $\omega^2(k)$. Then we seek $d_k^n u \in H_{x_1\text{-per}}^1(C)$ and $\lambda \in \mathbb{C}$ such that

$$\begin{aligned} & \int_C \alpha(\nabla + ika_1) d_k^n u \cdot (\nabla - ika_1) \bar{v} - \omega^2 \beta d_k^n u \bar{v} \, dx - \int_{\Gamma_T} \alpha \Lambda^T(\omega, k) d_k^n u \bar{v} \, ds(\mathbf{x}) \\ & - \int_{\Gamma_B} \alpha \Lambda^B(\omega, k) d_k^n u \bar{v} \, ds(\mathbf{x}) + \lambda \int_C \nabla u \cdot \nabla \bar{v} + u \bar{v} \, dx = f_n^{\text{DtN}}(v), \\ & \int_C \nabla d_k^n u \cdot \nabla \bar{u} + d_k^n u \bar{u} \, dx = 0, \end{aligned}$$

for all $v \in H_{x_1\text{-per}}^1(C)$.

The formula (B.5) is very technical and looks complicated. However, recall that we sketched above a scheme to compute the total derivatives $\frac{d^n \Lambda^{T/B}}{dk^n}$, $\frac{d^n \Lambda_\omega^{T/B}}{dk^n}$ and $\frac{d^n \Lambda_k^{T/B}}{dk^n}$ for all $n \in \mathbb{N}$. With these derivatives at hand, Eq. (B.5) is only slightly more complicated than the formula (3.5) for the n -th derivative of the dispersion curves in the case without DtN operators.

Acknowledgments

We would like to thank the reviewers for their extensive reports that helped to improve the manuscript significantly. This work was supported by the DFG Research Center MATHEON “Mathematics for key technologies”, project D26.

References

- [1] I. Babuška and J. Osborn. Eigenvalue problems. *Handbook of Numerical Analysis*, II:641–787, 1991.
- [2] D. Boffi, M. Conforti, and L. Gastaldi. Modified edge finite elements for photonic crystals. *Numer. Math.*, 105(2):249–266, 2006.
- [3] H. Brandsmeier. Standard and generalized hp-finite element discretizations for periodic structures. PhD thesis, ETH Zurich, 2013.
- [4] H. Brandsmeier, K. Schmidt, and C. Schwab. A multiscale hp-FEM for 2D photonic crystal bands. *J. Comput. Phys.*, 230(2):349–374, 2011.
- [5] L. Brillouin. *Wave Propagation and Group Velocity*. Pure and Applied Physics, Vol. 8. Academic Press, New York, NY, USA, 1960.
- [6] K. Busch. Photonic band structure theory: Assessment and perspectives. *C. R. Physique*, 3(1):53–66, 2002.
- [7] C. Carstensen, J. Gedicke, V. Mehrmann, and A. Miedlar. An adaptive homotopy approach for non-selfadjoint eigenvalue problems. *Numer. Math.*, 119(3):557–583, 2011.

- [8] Concepts Development Team. Webpage of Numerical C++ Library Concepts 2. <http://www.concepts.math.ethz.ch>, 2013.
- [9] C. M. de Sterke and J. E. Sipe. Envelope-function approach for the electrodynamics of non-linear periodic structures. *Phys. Rev. A*, 38:5149–5165, 1988.
- [10] C. Engström and M. Richter. On the spectrum of an operator pencil with applications to wave propagation in periodic and frequency dependent materials. *SIAM J. Appl. Math.*, 70(1):231–247, 2009.
- [11] S. Fliss. A Dirichlet-to-Neumann approach for the exact computation of guided modes in photonic crystal waveguides. *SIAM J. Sci. Comput.*, 35(2):B438–B461, 2013.
- [12] P. Frauenfelder and C. Lage. Concepts – an object-oriented software package for partial differential equations. *Math. Model. Numer. Anal.*, 36(5):937–951, 2002.
- [13] S. Giani and I. G. Graham. Adaptive finite element methods for computing band gaps in photonic crystals. *Numer. Math.*, 121(1):31–64, 2012.
- [14] D. Hermann, M. Frank, K. Busch, and P. Wölfe. Photonic band structure computations. *Opt. Express*, 8(3):167–172, 2001.
- [15] V. Hoang, M. Plum, and C. Wieners. A computer-assisted proof for photonic band gaps. *Z. Angew. Math. Phys.*, 60(6):1035–1052, 2009.
- [16] Z. Hu and Y. Y. Lu. Improved Dirichlet-to-Neumann map method for modeling extended photonic crystal devices. *Opt. Quantum Electron.*, 40(11-12):921–932, 2008.
- [17] E. Istrate, A. A. Green, and E. H. Sargent. Behavior of light at photonic crystal interfaces. *Phys. Rev. B*, 71(19):195122, 2005.
- [18] W. Jiang, R. T. Chen, and X. Lu. Theory of light refraction at the surface of a photonic crystal. *Phys. Rev. B*, 71:245115, 2005.
- [19] J. D. Joannopoulos. *Photonic Crystals: Molding the Flow of Light*. Princeton University Press, Princeton, NJ, USA, 2008.
- [20] P. Kaspar, R. Kappeler, D. Erni, and H. Jäckel. Average light velocities in periodic media. *J. Opt. Soc. Am. B*, 30(11):2849–2854, 2013.
- [21] T. Katō. *Perturbation Theory for Linear Operators*. Grundlehren der Mathematischen Wissenschaften. Springer, Berlin & Heidelberg, Germany, 1995.
- [22] D. Klindworth, K. Schmidt, and S. Fliss. Numerical realization of Dirichlet-to-Neumann transparent boundary conditions for photonic crystal wave-guides. *Comput. Math. Appl.*, 67(4):918–943, 2014.
- [23] P. Kuchment. *Floquet Theory for Partial Differential Equations*. Birkhäuser, Basel, Switzerland, 1993.
- [24] P. Kuchment. *The Mathematics of Photonic Crystals*, chapter 7, pages 207–272. SIAM, Philadelphia, PA, USA, 2001.
- [25] S. Lui, H. Keller, and T. Kwok. Homotopy method for the large, sparse, real nonsymmetric eigenvalue problem. *SIAM J. Matrix Anal. Appl.*, 18(2):312–333, 1997.
- [26] M. Marletta and R. Scheichl. Eigenvalues in spectral gaps of differential operators. *J. Spectr. Theory*, 2(3):293–320, 2012.
- [27] R. A. Norton and R. Scheichl. Convergence analysis of planewave expansion methods for 2D Schrödinger operators with discontinuous periodic potentials. *SIAM J. Numer. Anal.*, 47(6):4356–4380, 2010.
- [28] R. A. Norton and R. Scheichl. Planewave expansion methods for photonic crystal fibres. *Appl. Numer. Math.*, 63(0):88 – 104, 2013.
- [29] F. Odeh and J. B. Keller. Partial differential equations with periodic coefficients and bloch waves in crystals. *Journal of Mathematical Physics*, 5(11):1499–1504, 1964.

- [30] S. Olivier, H. Benisty, C. J. M. Smith, M. Rattier, C. Weisbuch, and T. F. Krauss. Transmission properties of two-dimensional photonic crystal channel waveguides. *Opt. Quant. Electron.*, 34:171–181, 2002.
- [31] S. Olivier, M. Rattier, H. Benisty, C. Weisbuch, C. J. M. Smith, R. M. De La Rue, T. F. Krauss, U. Oesterle, and R. Houdre. Mini-stopbands of a one-dimensional system: The channel waveguide in a two-dimensional photonic crystal. *Phys. Rev. B*, 63(11):113311, 2001.
- [32] A. Quarteroni, R. Sacco, and F. Saleri. *Numerical Mathematics*, volume 37 of *Texts in Applied Mathematics*. Springer, Berlin & Heidelberg, Germany, 2nd edition, 2007.
- [33] M. Reed and B. Simon. *Methods of Modern Mathematical Physics, volume 4: Analysis of Operators*. Academic Press, New York, NY, USA, 1978.
- [34] S. Sauter and C. Schwab. *Boundary Element Methods*. Springer, Berlin & Heidelberg, Germany, 2011.
- [35] K. Schmidt and R. Kappeler. Efficient computation of photonic crystal waveguide modes with dispersive material. *Opt. Express*, 18(7):7307–7322, 2010.
- [36] K. Schmidt and P. Kauf. Computation of the band structure of two-dimensional photonic crystals with hp finite elements. *Comp. Meth. App. Mech. Engr.*, 198:1249–1259, 2009.
- [37] J. E. Sipe. Vector $k \cdot p$ approach for photonic band structures. *Phys. Rev. E*, 62(4):5672–5677, 2000.
- [38] S. Soussi. Convergence of the supercell method for defect modes calculations in photonic crystals. *SIAM J. Numer. Anal.*, 43(3):1175–1201, 2005.